Molecular link between auxin and ROS-mediated polar growth

Silvina Mangano[a,b,c,1], Silvina Paola Denita-Juarez[a,b,c,1], Hee-Seung Choi[d,1], Eliana Marzol[a,b,c,1], Youra Hwang[d], Philippe Ranocha[e], Silvia Melina Velasquez[a,b,c,2], Cecilia Borassi[a,b,c], María Laura Barberini[f], Ariel Alejandro Aptekmann[g], Jorge Prometeo Muschietti[f,h], Alejandro Daniel Nadra[g], Christophe Dunand[e], Hyung-Taeg Cho[d,3], and José Manuel Estevez[a,b,c,3]

[a]Fundación Instituto Leloir, Buenos Aires C1405BWE, Argentina; [b]IIBBA-CONICET, Buenos Aires C1405BWE, Argentina; [c]Instituto de Fisiología, Biología Molecular y Neurociencias, IFIByNE-CONICET, Facultad de Ciencias Exactas y Naturales, Universidad de Buenos Aires, Ciudad Universitaria, Buenos Aires C1428EGA, Argentina; [d]Department of Biological Sciences, Seoul National University, Seoul 151-742, Korea; [e]Laboratoire de Recherche en Sciences Végétales, Université de Toulouse, Université Paul Sabatier, UMR 5546, CNRS, F-31326 Castanet-Tolosan, France; [f]Instituto de Investigaciones en Ingeniería Genética y Biología Molecular, Dr. Héctor Torres, INGEBI-CONICET, Buenos Aires 1428, Argentina; [g]Departamento de Química Biológica, IQUIBICEN-CONICET, Facultad de Ciencias Exactas y Naturales, Universidad de Buenos Aires, Ciudad Universitaria, Buenos Aires C1428EGA, Argentina; and [h]Departamento de Biodiversidad y Biología Experimental, Facultad de Ciencias Exactas y Naturales, Universidad de Buenos Aires, Ciudad Universitaria, Buenos Aires C1428EGA, Argentina

Root hair polar growth is endogenously controlled by auxin and sustained by oscillating levels of reactive oxygen species (ROS). These cells extend several hundred-fold their original size toward signals important for plant survival. Although their final cell size is of fundamental importance, the molecular mechanisms that control it remain largely unknown. Here we show that ROS production is controlled by the transcription factor RSL4, which in turn is transcriptionally regulated by auxin through several auxin response factors (ARFs). In this manner, auxin controls ROS-mediated polar growth by activating RSL4, which then up-regulates the expression of genes encoding NADPH oxidases (also known as RESPIRATORY BURST OXIDASE HOMOLOG proteins) and class III peroxidases, which catalyze ROS production. Chemical or genetic interference with ROS balance or peroxidase activity affects root hair final cell size. Overall, our findings establish a molecular link between auxin and ROS-mediated polar root hair growth.

auxin | root hair growth | RSL4 | ROS | peroxidases

In *Arabidopsis thaliana*, root hair cells and non-hair cell layers differentiate from the epidermis in the meristematic zone of the root. Once root hair cell fate has been determined, root hairs protrude from the cell surface and represent up to 50% of the surface root area; this process is crucial for nutrient uptake and water absorption. Root hair growth is controlled by the interplay of several proteins, including the transcription factor (TF) ROOT HAIR DEFECTIVE 6 (RHD6), a class I RSL protein belonging to the basic helix–loop–helix (bHLH) family (1). The bHLH transcription factor RSL4 (ROOT HAIR DEFECTIVE SIX-LIKE 4), which defines the final root hair length based on its level of expression (2), is a central growth regulator acting downstream of RHD6. Other TFs also contribute to the regulation of root hair growth (3, 4). Root hair cell elongation is modulated by a wide range of both environmental signals (5, 6) and endogenous hormones, such as ethylene and auxin (2, 5, 7). However, the underlying mechanisms are unknown. The transcriptional auxin response is mediated by auxin binding to receptors of the TRANSPORT INHIBITOR RESPONSE 1/AUXIN SIGNALING F-BOX (TIR1/AFB) family and its coreceptor AUXIN/INDOLE 3-ACETIC ACID (Aux/IAA). This triggers the proteasome-dependent degradation of Aux/IAA, which results in the release of the auxin response factors (ARFs). The released ARFs bind to *cis*-auxin response elements (Aux-REs) in the promoters of early auxin response genes to trigger downstream responses (8). Gain-of-function mutants for several Aux/IAAs exhibit reduced root hair growth (9). On the other hand, a high degree of genetic redundancy is expected in root hairs because several ARFs are highly expressed in trichoblast cells [e.g., ARF7 and

ARF19 are the two most abundant ARFs (10)]. In agreement, the *arf7arf19* double mutant did not show a reduction in root cell elongation (11), indicating that there are other ARFs acting downstream of auxin in growing root hair cells. Auxin needs to be sensed in situ in hair cells to trigger cell expansion, although no molecular connection has been proposed yet between ARFs and downstream TFs that control growth (*SI Appendix*, Fig. S1). Downstream auxin signaling is sustained by an oscillatory feedback loop composed of two main components, calcium ions (Ca^{2+}) and reactive oxygen species (ROS). High levels of cytoplasmic Ca^{2+} ($_{cyt}Ca^{2+}$) trigger ROS production by RBOHs (RESPIRATORY BURST OXIDASE HOMOLOG proteins), and high levels of $_{apo}$ROS activate unknown Ca^{2+}-permeable channels that promote Ca^{2+} influx into the cytoplasm (12, 13). Plant RBOHs are plasma membrane-localized NADPH oxidases that produce apoplastic superoxide ion (O_2^-), which is mostly converted chemically or enzymatically into hydrogen peroxide (H_2O_2). *Arabidopsis* RBOHs

Significance

Tip-growing root hairs are an excellent model system for deciphering the molecular mechanism underlying reactive oxygen species (ROS)-mediated cell elongation. Root hairs are able to expand in response to external signals, increasing several hundred-fold their original size, which is important for survival of the plant. Although their final cell size is of fundamental importance, the molecular mechanisms that control it remain largely unknown. In this study, we propose a molecular mechanism that links the auxin–auxin response factors module to activation of RSL4, which directly targets genes encoding ROS-producing enzymes such as NADPH oxidases (or RESPIRATORY BURST OXIDASE HOMOLOG proteins) and secreted type III peroxidases. Activation of these genes impacts on apoplastic ROS homeostasis, thereby stimulating root hair cell elongation.

(AtRBOHA–J) are associated with diverse ROS-related growth responses (14–16); for instance, RBOHC promotes root hair budding (17, 18), and RBOHH,J are required for proper pollen tube growth (19). In addition, the pool of $_{apo}$ROS can be modulated by the activity of class III peroxidases (PERs) (20). The mechanism that links auxin to ROS-mediated cell growth is unclear (*SI Appendix*, Fig. S1). Here we propose a molecular mechanism in which endogenous auxin activates several ARFs to up-regulate the expression of *RSL4*, which controls ROS-mediated polar root hair growth by promoting the expression and activity of RBOH and PER proteins. On the other hand, we were not able to detect an auxin-mediated nontranscriptional fast response to trigger ROS production in root hair cells.

Results and Discussion

Several ARFs Mediate RSL4 Activation, Linking Auxin-Dependent Polar Growth to ROS Production in Root Hair Cells. To establish whether ROS production is linked to auxin-dependent polar growth, we analyzed root hair growth and ROS levels in the presence of exogenously supplied auxin (100 nM IAA). Auxin enhances root hair growth (Fig. 1*A* and *SI Appendix*, Fig. S2*A*) and triggers a slightly higher ROS level in root hairs longer than 300 μm (*SI Appendix*, Fig. S2*B*). Next, we monitored cytoplasmic H_2O_2 ($_{cyt}H_2O_2$) levels using a genetically encoded YFP-based H_2O_2 sensor, named HyPer, which reacts with H_2O_2 when external $_{apo}H_2O_2$ is applied in the growing tip (*SI Appendix*, Fig. S3*A*). H_2O_2 levels in auxin-treated roots maintain a moderate HyPer signal in root hairs longer than 700 μm, whereas there is no root hair development in nontreated ones that reach these cell lengths (*SI Appendix*, Fig. S3*B*). Hence, the maintenance of $_{cyt}$ROS levels is a reliable response to auxin in tip-growing root hairs. Auxin triggers polar root hair growth via an unknown mechanism involving RSL4 activation (5). First, we analyzed whether both RSL2 and RSL4 directly regulate ROS production to trigger root hair growth. The *rsl2-1 rsl4-1* double mutant showed highly reduced ROS levels, whereas slightly higher ROS levels were detected in the RSL4-overexpressing line (RSL4^{OE}) than in the wild type (WT) during late stages of root hair development (≥400 μm in length) (Fig. 1 *B* and *C*). Therefore, both active RSL2 and RSL4 stimulate ROS production (Fig. 1*C* and *SI Appendix*, Fig. S2*D*). We then tested whether auxin triggers ROS production in an RSL2/RSL4-dependent manner. Auxin partially stimulated root hair growth and ROS production in each of the *rsl4-1* and *rsl2-1* null mutants but failed in the *rsl2-1 rsl4-1* double mutant (Fig. 1 *A* and *B* and *SI Appendix*, Fig. S2 *C* and *D*). Mutants for other reported TFs involved in root hair growth, such as *mamyb* (3) and *hdg11* (4), were treated with auxin, but normal responses were observed, suggesting that these TFs are not involved in auxin activation (*SI Appendix*, Fig. S4). In addition, the RSL4^{OE} line was less sensitive to the RBOH inhibitor VAS2870 (VAS) with respect to cell growth-linked ROS production (*SI Appendix*, Fig. S5). Overall, these findings highlight the key role of both RSL2 and RSL4, although RSL4 has a more protagonist role as a main transcriptional activator of the ROS-related auxin response in root hairs.

Next, we tested whether ARFs regulate root hair growth by up-regulating RSL4 expression and ROS production. Several ARFs, such as ARF5, ARF7, ARF8, and ARF19, are expressed in the meristematic and elongation zones of the root as well as in trichoblast cells and developing root hairs (*SI Appendix*, Fig. S6 *A and B*). Based on the lack of phenotype for the *arf7 arf19* mutant (11), all data suggest a high degree of functional redundancy between these ARFs possibly involved in root hair growth. To overcome this, we then generated lines overexpressing these ARFs under the control of the strong root hair-specific promoter EXPA7 ($_{P7}$:ARF; *SI Appendix*, Fig. S6*C*). Root hair growth was enhanced in three overexpression lines tested, especially in the ARF5 line (Fig. 1*D* and *SI Appendix*, Fig. S6*C*). Furthermore, RSL4 expression was elevated
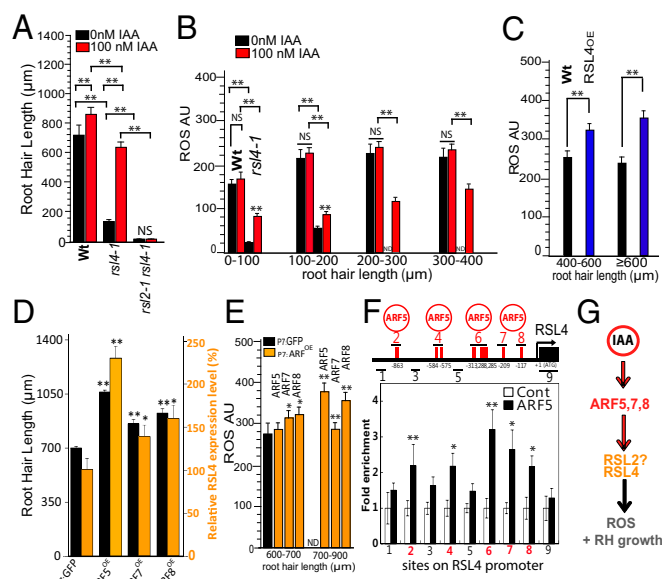
Fig. 1. ARF-mediated RSL4 activation links auxin-dependent polar root hair growth to ROS production. (*A*) Root hair length (mean ± SD) in WT Col-0, *rsl4-1*, and *rsl2-1 rsl4-2* treated with 100 nM IAA. (*B*) Effect of auxin (100 nM IAA) mediated by RSL4 on ROS production. ROS signal analysis with IAA treatment of WT Col-0 and the *rsl4-1* mutant in the early stages of root hair development. AU, fluorescent arbitrary units. (*C*) ROS in WT Col-0 and the RSL4 overexpressor in later stages of root hair growth. (*D*) Effect of EXP7 (EXPANSIN 7)-driven ARF5 ($_{P7}$:ARF5^{OE}), ARF7 ($_{P7}$:ARF7^{OE}), and ARF8 ($_{P7}$:ARF8^{OE}) overexpression on polar root hair growth (black bars) and RSL4 expression (orange bars) (mean ± SD). (*E*) ROS in EXP7-GFP/WT Col-0 ($_{P7}$:GFP as control) and the EXP7-driven ARF5,7,8 ($_{P7}$:ARF5,7,8^{OE}) overexpressor in the later stages of root hair development. (*F*) ChIP analysis showing ARF5 binding to auxin response elements on the RSL4 promoter region. The RSL4 promoter region (pRSL4) and the relative positions of Aux-REs (red bars) and ChIP-PCR regions (lines 1 to 9) are indicated. (*Bottom*) The enrichment fold of ARF5-GFP in ChIP-PCR of each region shown. Cont, control, empty vector line; ARF5, pMDC7:ARF5-GFP, dexamethasone-inducible ARF5-GFP line. The values are relative to each Cont value and significantly different (**$P < 0.001$, *$P < 0.005$; t test) from each Cont value. (*G*) Proposed events from the IAA signal mediated by ARF5 activation of *RSL4* expression to ROS-linked root hair (RH) growth. (*A–E*) One-way ANOVA; **$P < 0.001$, *$P < 0.01$. ND, not detected; NS, not significantly different. Error bars indicate ± SD of biological replicates.

(Fig. 1*D*) and high ROS levels were maintained in the root hair cells of these lines during late developmental stages (Fig. 1*E*). Given that the region upstream of RSL4 contains eight ARF response elements (Fig. 1*F* and *SI Appendix*, Table S2), we speculated that these ARFs would be able to bind to the RSL4 promoter and trigger its expression. To test this possibility, we carried out chromatin immunoprecipitation (ChIP) analyses (Fig. 1*F*) using an estradiol-inducible version of ARF5-GFP because it was the most efficient ARF tested to up-regulate *RSL4* expression. ChIP of ARF5 showed that the fold-enrichment levels are significantly higher in the Aux-RE regions than in the control (Fig. 1*F*). These data indicate that ARF5 binds to Aux-REs in the RSL4 promoter region and positively regulates its expression. It is highly possible that ARF7 and ARF8 also bind and regulate *RSL4* expression. Previously, it was shown that the Aux/IAA14 *slr-1* resistant mutant lacked root hairs (9), suggesting a strong inhibition of these ARFs. To test whether a single ARF is able to overcome this inhibition, we selected ARF19 because it is one of the ARFs most highly expressed in root hair cells (10). High levels of ARF19 (ARF19^{OE}; overexpression) were transgenically expressed in the Aux/IAA14 *slr1-1* root hair-less background. ARF19^{OE} was able to completely rescue the *slr1-1* root hair phenotype and normalize ROS levels (*SI Appendix*, Fig. S7 *A and*

Mangano et al.

B). As expected, ARF19 nuclear expression is highly responsive to auxin and is localized in root epidermal cells close to the root hair development zone (*SI Appendix*, Figs. S6*B* and S7*C*). Together, these results and previous reports (9–11) suggest that high auxin levels in trichoblast cells would release several ARFs (e.g., ARF5, ARF7, ARF8, and ARF19) from its repressors Aux/IAAs, to directly control RSL4 expression (and possibly RSL2), triggering ROS-mediated root hair elongation (Fig. 1*F*). Further experiments are required to establish how these ARFs are regulated to act in a coherent manner to trigger the transcriptional response during cell growth.

RSL4-Regulated *RBOHC,J* as Well as *RBOHH* Drive ROS-Mediated Root Hair Growth. Besides RBOHC, two other RBOH groups exist: One group clusters RBOHC and is composed of RBOHE,F (*SI Appendix*, Fig. S8*A*), and the other was previously implicated in polar growth of pollen tubes (19) and is composed of RBOHH,J. To identify which of these RBOHs also contribute to ROS-linked tip growth, we isolated *rboh* mutants (*SI Appendix*, Fig. S8*B* and Table S1) and screened them for abnormal cell expansion linked to deficient ROS production (Fig. 2 *A* and *B*). Only *rbohc-1* and *c-2* showed short root hairs, whereas *rbohh-1* and *h-3* developed slightly less elongated cells (*SI Appendix*, Fig. S8 *C* and *D*). When double *rboh* mutants were analyzed, only *rbohh,j* and mutants containing *rbohc* showed a clear root hair growth reduction of up to 40% (Fig. 2*A*). In agreement with this, *rbohc* mutants showed highly reduced ROS levels, whereas double *rbohh,j* mutants presented moderate to low ROS levels (Fig. 2*B* and *SI Appendix*, Fig. S8 *E* and *F*). We then used the HyPer H₂O₂ sensor to test whether the RBOH inhibitor VAS could limit the level of $_{cyt}H_2O_2$ in the growing root hair tip. The level of $_{cyt}H_2O_2$ was significantly diminished after VAS treatment (Fig. 2*C*), and $_{cyt}H_2O_2$ signatures were drastically modified in *rbohc-1* root hairs (Fig. 2*D*). Exogenous H₂O₂ treatment failed to rescue the *noxc-1* root hair growth defect (*SI Appendix*, Fig. S9*A*), implying that a complex and fine-tuned ROS regulation would be required to trigger growth. Together, these data suggest that although RBOHC is the main RBOH involved in ROS-mediated root hair growth, as reported previously (12, 17), RBOHH,J are also important ROS-producing enzymes in this process.

Based on an analysis of RSL4-regulated genes (5), a putative RSL4 response element (RSL4-RE) with the sequence TN₆CA[CT]G[TA] was identified that is highly similar to the root hair *cis*-element (RHE) TN₅₋₆CACG[TA]. The promoter regions of the *RBOHC, H*, and *J* genes include several RHEs, suggesting that these three RBOHs could be direct targets of the RSL4 TF (*SI Appendix*, Table S2). Using ChIP analysis, we examined whether RSL4-GFP could bind to the promoter regions of RBOHC,H,J in vivo. Except for the RBOHH gene, RSL4 bound to at least one RHE region in the RBOHC and RBOHJ promoters (Fig. 2*E*). This result suggests that RSL4 directly regulates these two ROS-related genes to generate the ROS required for tip growth.

Why are three RBOH proteins needed to trigger polar growth in a single cell? The simplest hypothesis is that these RBOHs act sequentially. Low levels of ROS were detected when the root hair first emerged from the root, but the ROS signal was up to twofold greater in slightly longer WT Col-0 root hairs (of 200 to 250 μm in length) (*SI Appendix*, Fig. S9 *D* and *E*). At a comparable stage, root hairs of the *rbohc-1* mutant had very low levels of $_{cyt}$ROS and those of the *rbohh,j* double mutant had only slightly lower ROS levels than did those of WT Col-0. In later growth stages, $_{cyt}$ROS levels were drastically reduced in the double *rbohh,j* mutant. This suggests that RBOHC is the first RBOH to produce ROS, and that RBOHC functionally overlaps with RBOHH,J. Finally, RBOHH,J produced ROS that was linked to root hair tip elongation at later developmental stages (>200 μm in length) (*SI Appendix*, Fig. S9*E*). Next, we investigated whether ROS is required for root hair initiation by subjecting WT Col-0 roots to
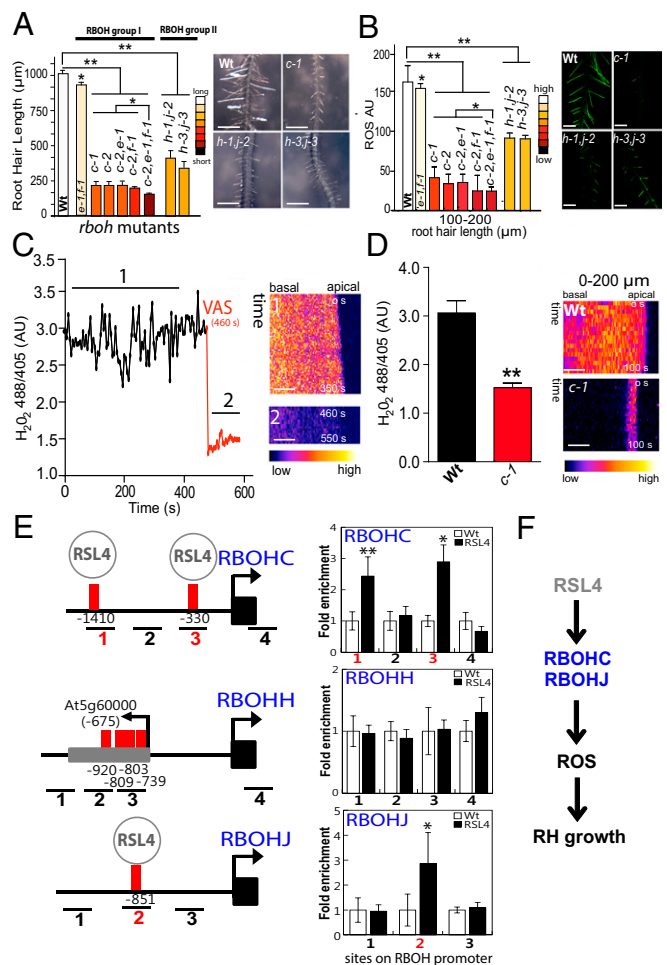
Fig. 2. RSL4-regulated *RBOHC, J*, as well as *H* drive ROS-mediated root hair growth. (*A*, *Right*) Root hair phenotype in WT Col-0 and *rboh* mutants. (Scale bars, 600 μm.) (*Left*) Root hair length (mean ± SD; n = 30 roots) in *rboh* mutants. (*B*) Total ROS generated by oxidation of H₂DCF-DA in early stages of root hair development in *rboh* mutants. (*Right*) Total ROS H₂DCF-DA staining in roots of WT Col-0 and *rboh* mutants. (Scale bars, 600 μm.) (*C*) $_{cyt}H_2O_2$ levels in VAS-treated WT Col-0 root hairs expressing the HyPer sensor. $_{cyt}H_2O_2$ levels are based on the ratio 488/405 nm of HyPer biosensor at the root hair tip over 600 s. (*Right*) Selected kymographs resulting from this analysis only for root hairs of >200 μm in length. (Scale bars, 5 μm.) (*D*) $_{cyt}H_2O_2$ average levels in *rbohc-1* and WT Col-0 root hairs expressing HyPer. Average $_{cyt}H_2O_2$ levels are based on the 488/405 nm ratio of HyPer at the root hair tip in root hairs of 0 to 200 μm in length. (*Right*) Selected kymographs. (Scale bars, 5 μm.) (*E*) Promoter regions of ROS-related genes *RBOHC, H*, and *J* as targets of the RSL4 response element (red bars) and ChIP-PCR regions (lines 1 to 4). Neighboring gene exons are indicated as a gray box. Enrichment fold of RSL4-GFP in ChIP-PCR for each region shown. RSL4, $_{pRSL4}$:RSL4-GFP. Error bars indicate ± SD of biological replicates (n = 2). The values are relative to each Cont value. Significantly different (**P < 0.01, *P < 0.05; *t* test) from the Cont value. (*F*) Proposed events from RSL4 activation of RBOHC,J to ROS-mediated polar root hair growth. (*A*, *B*, and *D*) One-way ANOVA; **P < 0.001, *P < 0.01. Error bars indicate ± SD of biological replicates.

VAS. The concentration of VAS needed to inhibit root hair growth by half (IC₅₀) was ~7.5 μM (*SI Appendix*, Fig. S9*B*), which is similar to ROS VAS IC₅₀ (~7.0 μM) (*SI Appendix*, Fig. S9*C*). The *rbohc-1* mutant (12) showed very short root hairs up to 150 μm in length (*SI Appendix*, Fig. S9*B*) but still produced ~30% of ROS compared with WT root hairs (Fig. 2*D* and *SI Appendix*, Fig. S9*C*), indicating the presence of residual ROS production (17). Because ROS homeostasis could be modified by the activity of PER, we treated WT and *rbohc-1* mutant roots with the PER

inhibitor SHAM (salicylhydroxamic acid) (21) at concentrations of up to 100 μM. SHAM treatment resulted in a significant reduction in total ROS in *rbohc-1* in comparison with nontreated *rbohc-1*, although root hair initiation was not abolished (*SI Appendix*, Fig. S10). In an analysis using HyPer, 100 μM SHAM completely abolished the H_2O_2 signal in the whole root (*SI Appendix*, Fig. S11), confirming that PERs also contribute to ROS production. This implies that, at least in *A. thaliana*, initial development of the root hair tip is not affected by highly reduced ROS levels.

RSL4-Regulated *PER*s Affect ROS Homeostasis and Polar Root Hair Growth.

Next, coexpression analysis revealed that *RSL4* is highly coregulated at the transcriptional level with several *PER* genes, most of which exhibit root hair expression (*SI Appendix*, Fig. S12 *A* and *B*) (5). We then analyzed the corresponding T-DNA *per* mutants (*SI Appendix*, Fig. S12*C* and Table S1). The single mutant *per1-2* and double mutant *per44-2,73-3* (all null mutants except for *per1-2* knockdown; *SI Appendix*, Fig. S12*D*) showed mild phenotypes (short root hairs), with up to ~30% reductions in ROS levels (Fig. 3 *A* and *B*). This suggests that there is genetic redundancy between these PERs in the regulation of ROS homeostasis. The levels of $_{cyt}H_2O_2$, as visualized with HyPer, were reduced in root hairs treated with 75 μM SHAM (Fig. 3*C*), and this result was confirmed using a 2′, 7′-dichlorodihydrofluorescein diacetate (H_2DCF-DA) probe (*SI Appendix*, Fig. S10*B*). In addition, peroxidase activity was significantly lower in SHAM-treated roots as well as in *per* mutants and higher in PER44 overexpressor (PER44^OE) than in WT nontreated ones (Fig. 3*D*), suggesting a direct link between peroxidase activity and ROS homeostasis. To explore the transcriptional regulation of these *PER*s in ROS-mediated root hair growth, we analyzed the regulatory region of the genes encoding these *PER*s. We identified several putative RHE motifs (*SI Appendix*, Table S3), suggesting that these genes could be direct targets of RSL4, as suggested by the coexpression analysis (*SI Appendix*, Fig. S12*A*). ChIP assays revealed that RSL4 binds to the RHE of four *PER*s, *PER1*, *44*, *60*, and *73* (Fig. 3*E*). In agreement with this, much higher and lower levels of *PER1* and *PER73* were detected in RSL4^OE/WT and WT/*rsl4-1* lines, respectively (5), suggesting that RSL4 promotes the expression of at least these two *PER*s. At last, higher peroxidase activity was found in _P7:ARF5 and _P7:ARF8 lines (where RSL4 expression is up-regulated; Fig. 1*D*) and much lower activity was detected in *rsl4-1*, which lacks RSL4 (Fig. 3*F*), confirming that RSL4 not only directs *PER* expression at the transcriptional level but also impacts on the PER activity (Fig. 3*G*).

We then examined whether auxin treatment could compensate for the lack of RBOH and PER proteins (Fig. 4 *A* and *B*). Auxin treatment partially rescued the reduced length and ROS levels of the *rbohc-1* mutant, resulting in ~30% increases in both, and almost fully rescued the defects in the *rbohh,j* and *per44-2,73-3* mutants (Fig. 4 *A* and *B*). When 15 μM VAS was added along with the auxin (IAA), the *rbohc-1* mutant exhibited intermediate root hair growth and partial recovery of ROS levels (*SI Appendix*, Fig. S13 *A* and *B*), suggesting other sources of ROS. When SHAM was added in addition to VAS (SHAM+VAS) in the presence of auxin, a low recovery of root hair growth and ROS levels was detected in *rbohc-1* and WT root hairs (*SI Appendix*, Fig. S13 *C* and *D*). Together, these findings confirm that auxin requires both RBOH-derived ROS and ROS produced by PER to modulate polar growth (*SI Appendix*, Fig. S13*E*). The small although detectable recovery in ROS and cell growth after auxin treatment in root hair cells (in *rbohc-1* as well as in WT) in the presence of both inhibitors, VAS and SHAM (*SI Appendix*, Fig. S13 *C* and *D*), would possibly suggest the existence of an unknown source of ROS coming from other apoplastic ROS-producing enzymes (e.g., oxalate oxidase, diamine oxidase, lipoxigenases, etc.) also regulated
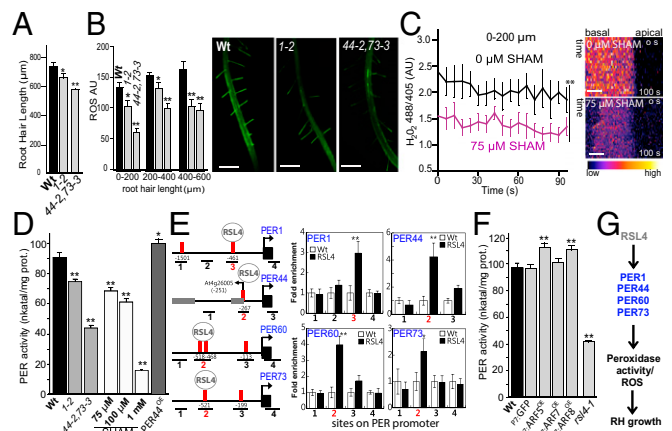

Fig. 3. RSL4-regulated *PER*s affect ROS homeostasis and polar root hair growth. (*A*) Root hair length (mean ± SD; *n* = 30 roots) in the single mutant *per1-2* and double mutant *per44-2,73-3*. (*B*) ROS in root hairs of the single mutant *per1-2* and double mutant *per44-2,73-3*. (*Right*) ROS H_2DCF-DA staining in roots of WT Col-0 and *per* mutants. (Scale bars, 600 μm.) (*C*) Average $_{cyt}H_2O_2$ levels in SHAM-treated and nontreated WT Col-0 root hairs expressing the HyPer sensor (*n* = 10). Average $_{cyt}H_2O_2$ levels are based on the 488/405 nm ratio of HyPer at the root hair tip over 100 s. One-way ANOVA; **$P < 0.001$. (*Right*) Selected kymographs. (Scale bars, 5 μm.) (*D*) Peroxidase activity in the roots of WT, *per1-2*, *per44-2*, and *per73-3* simple mutants, *per44-2,73-3* double mutant, and wild-type root extracts with increasing concentrations of SHAM. Enzyme activity (expressed as *n* katal/mg protein) was determined by a guaiacol oxidation-based assay. Values are the mean of three replicates ± SD. (*E*) Promoter regions of ROS-related genes PER1,44,60,73 showing the RSL4 response elements (red bars) and ChIP-PCR regions (lines 1 to 4). Positions are relative to the start codon. Neighboring gene exons are indicated as gray boxes. Enrichment fold of RSL4-GFP in ChIP-PCR of each region is shown. RSL4, pRSL4:GFP. Error bars indicate ± SD of biological replicates (*n* = 2). The values are relative to each WT value and significantly different (**$P < 0.01$, *$P < 0.05$; *t* test). (*F*) Peroxidase activity in the roots of WT, EXP7-driven GFP (as control), ARF5 (_P7:ARF5^OE), ARF7 (_P7:ARF7^OE), and ARF8 (_P7:ARF8^OE) as well as in the *rsl4-1* mutant. Enzyme activity (expressed as *n* katal/mg protein) was determined by a guaiacol oxidation-based assay. Values are the mean of three replicates ± SD. (*G*) Proposed events from RSL4 activation of PER1,44,60,73 to ROS-linked root hair growth. (*A*, *B*, *D*, and *F*) One-way ANOVA, **$P < 0.001$, *$P < 0.01$. Error bars indicate ± SD of biological replicates.

by auxin-RSL4 (and possibly RSL2) (*SI Appendix*, Fig. S13*E*), which will require further investigation.

Finally, we tested whether auxin is able to trigger a rapid and nontranscriptional response impacting on ROS production in the root hair tip (*SI Appendix*, Fig. S14). We applied IAA in growing root hairs that express the HyPer sensor, and no significant changes were detected before or after hormone treatment (*SI Appendix*, Fig. S14 *A* and *B*). A similar result was obtained when ROS levels were measured with the dye H_2DCF-DA (*SI Appendix*, Fig. S14*C*). Overall, our results suggest that the main auxin downstream targets are RSL4 (and possibly RSL2) and the transcriptional activation of genes related to ROS production and involved in polar growth (*SI Appendix*, Fig. S13*E*). We cannot exclude other direct nontranscriptionally activated targets involved in the auxin response in root hair cells, but we fail to detect changes in H_2O_2/ROS upon auxin stimulation in our experimental conditions.

Conclusions

A root hair is a single-cell protrusion able to extend in response to external signals, increasing several hundred-fold its original size, which is important for survival of the plant. Final root hair size has vital physiological implications, determining the surface area/volume ratio of the whole roots exposed to nutrient pools, thereby likely impacting nutrient uptake rates. Although the final hair size is of fundamental importance, the molecular mechanisms that
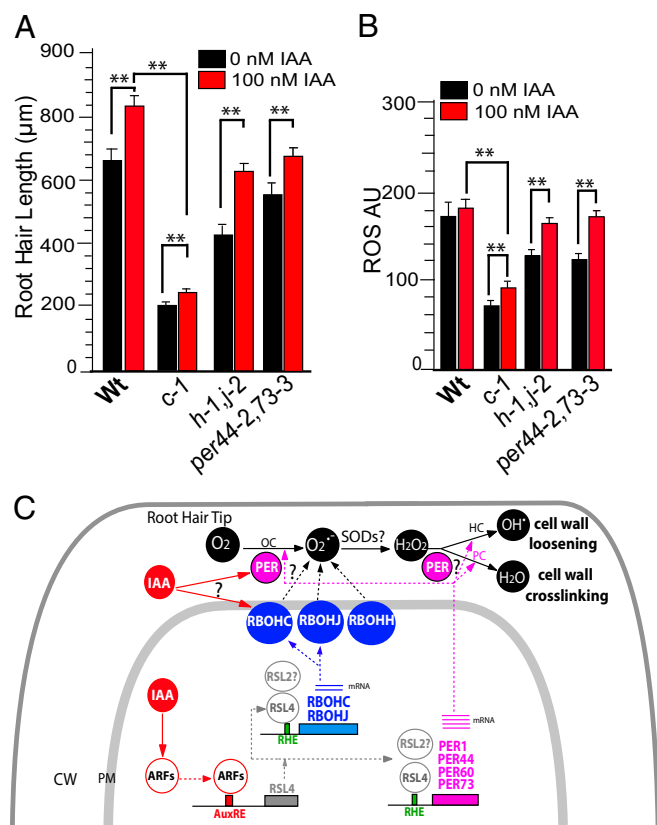
Fig. 4. Auxin-stimulated polar growth requires apoplastic ROS. (*A*) Root hair length (mean ± SD; $n = 30$ roots) in WT Col-0 and *rboh* and *per* mutants treated or not with 100 nM IAA. (*B*) ROS signal in WT and *rboh* mutants treated or not with 100 nM IAA. Root hairs of 0 to 200 μm in length were analyzed. (*C*) Model of auxin/ARF5/RSL4 regulation of ROS-mediated polar root hair growth. The bHLH transcription factor RSL4 is transcriptionally activated by auxin (IAA) and its expression is directly regulated by several ARFs (e.g., ARF5,7,8,19). Through RSL4 (and possibly RSL2), auxin activates the expression of two RBOHs (RBOHC,J) and four PERs (PER1,44,60,73) that together regulate ROS homeostasis in the apoplast (in combination with RBOHH). PERs in the presence of $_{apo}$ROS would control cell-wall loosening (in the peroxidative cycle; PC) and cross-linking reactions (in the hydroxylic cycle; HC) that impact on polar growth. PERs also contribute to the superoxide radical pool by oxidizing singlet oxygen (in the oxidative cycle; OC). Solid lines indicate activation or chemical conversion; dashed lines indicate protein translation and targeting or contribution. CW, cell wall; PM, plasma membrane. Reactive oxygen species: hydroxyl radical, $^\bullet OH$; superoxide ion, $O_2^{\bullet -}$; singlet oxygen, O_2; superoxide dismutases, SODs. ? indicates unidentified PER catalyzing the indicated reaction. (*A* and *B*) One-way ANOVA; **$P < 0.001$. Error bars indicate ± SD.

control it remain largely unknown. Here we propose a mechanism that explains how root hair tip growth works under auxin regulation of ROS homeostasis by activating several ARFs and subsequently up-regulating the expression of the bHLH TF RSL4 (and possibly RSL2). RSL2/RSL4-dependent ROS production is catalyzed by RBOH and PER enzymes, which facilitates polar root hair growth and defines its final cell size (Fig. 4*C*). Auxin is a prominent signal in trichoblast cells, and is essential for proper polar root hair growth. Auxin-ARF activation of the bHLH TF regulates several other plant developmental processes (22, 23). Here we have identified that auxin activates *RSL4* via several ARFs (ARF5,7,8), which bind (at least ARF5) to several Aux-REs (8) in the RSL4 regulatory region. In addition, high levels of ARF19 are able to overcome a resistant Aux/IAA14, s*lr1-1*, to trigger ROS-mediated polar growth. Recently, two dominant mutated versions of Aux/IAA7 were found to completely suppress

root hair growth by down-regulating RSL4 expression (24). Based on these results, we hypothesize that IAA7–IAA14 directly repress several ARFs (ARF5,7,8,19) to control RSL4 (and RSL2) expression. Based on the mutant analysis, RSL2 would act together with RSL4 to trigger ROS responses when stimulated with auxin. Once RSL4 is active, it will trigger RSL2 expression (2, 5), and both are able to control ROS homeostasis during polar root hair growth by directly regulating the expression of *RBOHs* and *PERs*. Different types of ROS affect cell growth by modulating the balance between cell proliferation and cell elongation in the root meristem (25, 26) by an unknown molecular mechanism. In this study, we report that, under auxin induction, RSL2/RSL4 triggers ROS-mediated cell elongation. ChIP analysis revealed that RSL4 directly regulates the expression of two *RBOHs* as well as four *PERs*. However, out of 34 putative direct targets of RSL4 reported (27), only a few (e.g., PER7) were found to be associated with ROS homeostasis. In another recent report, RSL4 was shown to bind to RHE and trigger (directly or indirectly) the expression of the smallest subset of 124 genes involved in ROS homeostasis, cell-wall synthesis and remodeling, metabolism, and signaling that are necessary and sufficient to trigger root hair growth (28). Still unknown are the RSL2 targets and how RSL2 acts in a cooperative way with RSL4. In addition, the transcriptional mediator subunit (MED) MED15/PHYTOCHROME AND FLOWERING TIME 1 affects ROS levels by triggering transcriptional changes in root hair cells (29), probably via a mechanism that does not involve RSL4. Alternatively, ROS homeostasis may be influenced by other factors, independent of the RSL4 transcriptional program, that also modulate RBOH and PER activities, such as Ca^{2+} binding and posttranslational modifications (18, 30). Overall, here we have established a key role of RSL4 as one transcriptional activator of the ROS-related auxin response in root hairs together with RSL2, but we cannot discard that other TFs could also act downstream of auxin and independent of RSL2/RSL4 to trigger ROS production in root hair cells (*SI Appendix*, Fig. S13E).

Here we identified two RBOHs (RBOHH and J) together with the previously reported RBOHC (12) and four PERs (PER1, 44, 60, and 73) that are involved in ROS-mediated polar root hair growth in *Arabidopsis* (Fig. 4*C*). In agreement with our findings, an RBOH named RTH5 (root hair-less 5) from maize with high sequence similarity to AtRBOHH,J was also linked to root hair cell expansion (31). Several of the PERs identified as contributing to ROS-mediated root hair growth were previously found to modulate cell growth but were not shown to be involved in ROS homeostasis (27, 32). Exogenously supplied H_2O_2 inhibited root hair polar expansion, whereas treatment with ROS scavengers (e.g., ascorbic acid) caused root hair bursting (16), reinforcing the notion that $_{apo}$ROS modulates cell growth by impacting cell-wall properties. In this manner, $_{apo}$ROS molecules ($_{apo}H_2O_2$) coupled to PER activity directly affect the degree of cell-wall crosslinking (14, 20) by oxidizing cell-wall compounds and leading to rigidification of the wall in peroxidative cycles (16). The identified PER1,44,60,73 directly contribute to PER activity in peroxidative cycles. On the other hand, $_{apo}$ROS coupled to PER activity enhances nonenzymatic wall loosening by producing oxygen radical species (e.g., $^\bullet OH$) and promoting polar growth in hydroxylic cycles (33). It is unclear how opposite effects on cell-wall polymers are coordinated during polar growth (20, 33). Finally, PERs also contribute to the superoxide radical ($O_2^{\bullet -}$) pool by oxidizing singlet oxygen in the oxidative cycle, thereby affecting $_{apo}H_2O_2$ levels. Although ROS is produced in the apoplast, influencing cell-wall properties during cell expansion, H_2O_2 is also present at high levels in the cytoplasm during polar growth (17). In agreement, H_2O_2 influx from the apoplast was demonstrated for several plant plasma membrane intrinsic proteins (PIPs) in heterologous systems (34, 35) as well as in plant cells (36). Because cytosolic acidification triggers a drastic reduction in the water permeability of several PIPs, it is plausible that oscillating pH changes in

PLANT BIOLOGY

growing root hairs (17) directly regulate the cycles of $_{cyt}H_2O_2$ influx. Once H_2O_2 molecules are transported into the cytoplasm, they trigger downstream responses linked to polar growth (12, 18).

Materials and Methods

Root Hair Phenotype. For quantitative analysis of root hair phenotypes in *rboh* mutants and WT Col-0, 200 fully elongated root hairs were measured (n = 30 roots) from seedlings grown on vertical plates for 10 d. Values are reported as the mean ± SD using ImageJ 1.50b software (NIH). Measurements made on images were captured with an Olympus SZX7 zoom microscope equipped with a Q-Color5 digital camera. Ten-day-old roots for ARF[OE] were digitally photographed with a stereomicroscope (M205 FA; Leica) at a 40× magnification. The hair length of 8 to 10 consecutive hairs protruded perpendicularly from each side of the root, for a total of 16 to 20 hairs from both sides of the root.

H_2DCF-DA Probe Used to Measure Total ROS. Growth of *Arabidopsis* seeds on a plate was done with 1% sterile agar for 8 d in a chamber at 25 °C with continuous light. These seedlings were incubated in darkness for 10 min with 50 μM 2′,7′-dichlorodihydrofluorescein diacetate at room temperature. Samples were observed with a confocal microscope equipped with a 488-nm argon laser and BA510IF filter sets. A 10× objective was used, 0.30 N.A., 4.7 laser intensity, 1.1 offset, 440 photomultiplier (PMT) (for highest ROS levels), 480 PMT (for ROS media), and gain 3. Images were taken scanning XZY with 2 μm between focal planes. Images were analyzed using ImageJ. To measure ROS highest levels, a circular region of interest (ROI) (r = 2.5) was chosen in the zone of the root hair with the highest intensities. To measure ROS mean, the total area of the root hair was taken. Pharmacological treatments were carried out with a combination of the following reagents: 100 nM and 5 μM IAA, 15 μM VAS2870, and 100 μM SHAM. In the case of a short time experiment with IAA, 8-d-old WT plants were incubated with 100 nM IAA for 3 min and coincubated for 7 min with 100 nM IAA and 50 μM H_2DCF-DA at room temperature. We washed the sample with MS 0.5× solution, and image acquisition was done with a 10× objective and 400 ms of exposure time on an epifluorescence microscope (Imager A2; Zeiss). As a control, we incubated 10-d-old WT plants with MS 0.5× solution for 3 min and coincubated for 7 min with MS 0.5× and 50 μM H_2DCF-DA at room temperature. To measure ROS levels, a circular ROI (r = 2.5) was taken at the tip of the root hair. Values are reported as the mean ± SD using ImageJ 1.50b software.

1. Menand B, et al. (2007) An ancient mechanism controls the development of cells with a rooting function in land plants. *Science* 316:1477–1480.
2. Datta S, Prescott H, Dolan L (2015) Intensity of a pulse of RSL4 transcription factor synthesis determines *Arabidopsis* root hair cell size. *Nat Plants* 1:15138.
3. Slabaugh E, Held M, Brandizzi F (2011) Control of root hair development in *Arabidopsis thaliana* by an endoplasmic reticulum anchored member of the R2R3-MYB transcription factor family. *Plant J* 67:395–405.
4. Xu P, et al. (2014) HDG11 upregulates cell-wall-loosening protein genes to promote root elongation in *Arabidopsis*. *J Exp Bot* 65:4285–4295.
5. Yi K, Menand B, Bell E, Dolan L (2010) A basic helix-loop-helix transcription factor controls cell growth and size in root hairs. *Nat Genet* 42:264–267.
6. Salazar-Henao JE, Schmidt W (2016) An inventory of nutrient-responsive genes in *Arabidopsis* root hairs. *Front Plant Sci* 7:237.
7. Song L, et al. (2016) The molecular mechanism of ethylene-mediated root hair development induced by phosphate starvation. *PLoS Genet* 12:e1006194.
8. Guilfoyle T, Hagen G, Ulmasov T, Murfett J (1998) How does auxin turn on genes? *Plant Physiol* 118:341–347.
9. Fukaki H, Tameda S, Masuda H, Tasaka M (2002) Lateral root formation is blocked by a gain-of-function mutation in the SOLITARY-ROOT/IAA14 gene of *Arabidopsis*. *Plant J* 29:153–168.
10. Bargmann BOR, et al. (2013) A map of cell type-specific auxin responses. *Mol Syst Biol* 9:688.
11. Okushima Y, et al. (2005) Functional genomic analysis of the *AUXIN RESPONSE FACTOR* gene family members in *Arabidopsis thaliana*: Unique and overlapping functions of ARF7 and ARF19. *Plant Cell* 17:444–463.
12. Foreman J, et al. (2003) Reactive oxygen species produced by NADPH oxidase regulate plant cell growth. *Nature* 422:442–446.
13. Wu J, et al. (2010) Spermidine oxidase-derived H_2O_2 regulates pollen plasma membrane hyperpolarization-activated Ca^{2+}-permeable channels and pollen tube growth. *Plant J* 63:1042–1053.
14. Lee Y, Rubio MC, Alassimone J, Geldner N (2013) A mechanism for localized lignin deposition in the endodermis. *Cell* 153:402–412.
15. Xie H-T, Wan Z-Y, Li S, Zhang Y (2014) Spatiotemporal production of reactive oxygen species by NADPH oxidase is critical for tapetal programmed cell death and pollen development in *Arabidopsis*. *Plant Cell* 26:2007–2023.
16. Orman-Ligeza B, et al. (2016) RBOH-mediated ROS production facilitates lateral root emergence in *Arabidopsis*. *Development* 143:3328–3339.
17. Monshausen GB, Bibikova TN, Messerli MA, Shi C, Gilroy S (2007) Oscillations in extracellular pH and reactive oxygen species modulate tip growth of *Arabidopsis* root hairs. *Proc Natl Acad Sci USA* 104:20996–21001.
18. Takeda S, et al. (2008) Local positive feedback regulation determines cell shape in root hair cells. *Science* 319:1241–1244.
19. Boisson-Dernier A, et al. (2013) ANXUR receptor-like kinases coordinate cell wall integrity with growth at the pollen tube tip via NADPH oxidases. *PLoS Biol* 11:e1001719.
20. Passardi F, Penel C, Dunand C (2004) Performing the paradoxical: How plant peroxidases modify the cell wall. *Trends Plant Sci* 9:534–540.
21. Brouwer KS, van Valen T, Day DA, Lambers H (1986) Hydroxamate-stimulated O(2) uptake in roots of *Pisum sativum* and *Zea mays*, mediated by a peroxidase: Its consequences for respiration measurements. *Plant Physiol* 82:236–240.
22. Schlereth A, et al. (2010) MONOPTEROS controls embryonic root initiation by regulating a mobile transcription factor. *Nature* 464:913–916.
23. Galli M, et al. (2015) Auxin signaling modules regulate maize inflorescence architecture. *Proc Natl Acad Sci USA* 112:13372–13377.
24. Lee M-S, An J-H, Cho H-T (2016) Biological and molecular functions of two ear motifs of *Arabidopsis* IAA7. *J Plant Biol* 59:24–32.
25. Tsukagoshi H, Busch W, Benfey PN (2010) Transcriptional regulation of ROS controls transition from proliferation to differentiation in the root. *Cell* 143:606–616.
26. Lu D, Wang T, Persson S, Mueller-Roeber B, Schippers JHM (2014) Transcriptional control of ROS homeostasis by KUODA1 regulates cell expansion during leaf development. *Nat Commun* 5:3767.
27. Vijayakumar P, Datta S, Dolan L (2016) ROOT HAIR DEFECTIVE SIX-LIKE4 (RSL4) promotes root hair elongation by transcriptionally regulating the expression of genes required for cell growth. *New Phytol* 212:944–953.
28. Hwang Y, Choi HS, Cho HM, Cho HT (2017) Tracheophytes contain conserved orthologs of a basic helix-loop-helix transcription factor that modulate ROOT HAIR SPECIFIC genes. *Plant Cell* 29:39–53.
29. Sundaravelpandian K, Chandrika NN, Schmidt W (2013) PFT1, a transcriptional Mediator complex subunit, controls root hair differentiation through reactive oxygen species (ROS) distribution in *Arabidopsis*. *New Phytol* 197:151–161.
30. Yun BW, et al. (2011) S-nitrosylation of NADPH oxidase regulates cell death in plant immunity. *Nature* 478:264–268.
31. Nestler J, et al. (2014) Roothairless5, which functions in maize (*Zea mays* L.) root hair initiation and elongation encodes a monocot-specific NADPH oxidase. *Plant J* 79:729–740.
32. Kwon T, et al. (2015) Transcriptional response of *Arabidopsis* seedlings during spaceflight reveals peroxidase and cell wall remodeling genes associated with root hair development. *Am J Bot* 102:21–35.
33. Dunand C, Crèvecoeur M, Penel C (2007) Distribution of superoxide and hydrogen peroxide in *Arabidopsis* root and their influence on root development: Possible interaction with peroxidases. *New Phytol* 174:332–341.
34. Dynowski M, Schaaf G, Loque D, Moran O, Ludewig U (2008) Plant plasma membrane water channels conduct the signalling molecule H_2O_2. *Biochem J* 414:53–61.
35. Miller EW, Dickinson BC, Chang CJ (2010) Aquaporin-3 mediates hydrogen peroxide uptake to regulate downstream intracellular signaling. *Proc Natl Acad Sci USA* 107:15681–15686.
36. Tian S, et al. (2016) Plant aquaporin AtPIP1;4 links apoplastic H_2O_2 induction to disease immunity pathways. *Plant Physiol* 171:1635–1650.

Supporting Information

The molecular link between auxin and ROS mediated polar root hair growth

Silvina Mangano, Silvina Paola Denita-Juarez, Hee-Seung Choi, Eliana Marzol, Youra Hwang, Philippe Ranocha, Silvia Melina Velasquez, Cecilia Borassi, María Laura Barberini, Ariel A. Aptekmann, Jorge Muschieti, Alejandro Daniel Nadra, Christophe Dunand, Hyung-Taeg Cho* & José Manuel Estevez*

* Correspondence should be addressed.
Email: htcho@snu.ac.kr (H-T.C.) and jestevez@leloir.org.ar (J.M.E).

This PDF file includes:

Materials and Methods
Fig. S1-S14
Table S1-S4
References (1-19)

Materials and Methods

Plant Growth and mutant isolation. *Arabidopsis thaliana* Columbia-0 (Col-0) was used as the wild type (Wt) genotype in all experiments, unless stated otherwise. All mutants and transgenic lines tested are in this ecotype. Seedlings were germinated on agar plates in a Percival incubator at 22°C in a growth room with 16h light/8h dark cycles for 10 days at 140 μmol m^{-2}s^{-1} light intensity. Plants were transferred to soil for growth under the same conditions as previously described at 22°C. For identification of T-DNA knockout lines, genomic DNA was extracted from rosette leaves. Confirmation by PCR of a single and multiple T-DNA insertions in the target RBOH and PER genes were performed using an insertion-specific LBb1 or LBb1.3 (for SALK lines) or Lb3 (for SAIL lines) primer in addition to one gene-specific primer. To ensure gene disruptions, PCR was also run using two gene-specific primers, expecting bands corresponding to fragments larger than in Wt. In this way, we isolated homozygous lines (for all the genes mentioned above). Mutant list is detailed in **SI Appendix, Table S1**.

HyPer sensor for measuring $_{cyt}$H$_2$O$_2$. HyPer consists of a circularly permuted YFP (cpYFP) molecule coupled to a regulatory domain of the *Escherichia coli* H$_2$O$_2$ sensor OxyR (1-4). When exposed to H$_2$O$_2$, the excitation peak of cpYFP shifts from 420 to 500 nm, while the emission peak remains at 516 nm (1) allowing it to be used as a ratiometric biosensor (2-4). Ten day-old *Arabidopsis* seedlings expressing the fluorescence HyPer biosensor were used. Root hairs were ratio imaged with the Zeiss LSM 510 laser scanning confocal microscope (Carl Zeiss) using a 40X oil-immersion, 1.2 numerical aperture. The HyPer biosensor was excited with both the 405 nm blue diode laser and with the 488 nm argon laser. The emission (516 nm) was collected using a primary dichroic mirror and the Meta-detector of the microscope. For time-lapse analysis, images were collected every 3s. To measure ROS highest levels, a circular ROI (r=2.5) was taken in the root hair tip for every imagen of the time lapse. Chemical treatments were made *in vivo* with 100 nM or 5 μM IAA, 50 μM of VAS 2970, 100 μM SHAM, and 10 mM H$_2$O$_2$. Values are reported as the mean ±SD using the Image J 1.50b software.

Chemical treatments. RBOH and PER and auxin treatment. Sterilized seeds were germinated on agar plates. After 5 days plants were transferred into a half-strength MS medium with 100 nM or 5 μM of indole-3-acetic acid (IAA) or/and 15 μM of VAS2870 (VAS, for 3-Benzyl-7-(2-benzoxazolyl)thio-1,2,3-triazolo(4,5-d)pyrimidine), or 100 μM SHAM or 10-500 μM H$_2$O$_2$. After 5 days (10 days old), quantitative analysis of root hair phenotypes and total ROS measurements with H$_2$DCF-DA were made.

Peroxidase activity. Soluble proteins were extracted from roots grown on vertical plates for 10 days by grinding in 20mM HEPES, pH 7.0, containing 1 mM EGTA, 10mM ascorbic acid, and PVP PolyclarAT (100mg g^{-1} fresh material; Sigma, Buchs, Switzerland). The extract was centrifuged twice for 10 min at 10000 g. Each extract was assayed for protein levels with the Bio-Rad assay (Bio-Rad) and for total peroxidase activity using guaïacol/H$_2$O$_2$. Enzyme activity

(expressed in nkatal/mg protein) was determined by a guaiacol oxidation-based assay. Values are the mean of three replicates ± SD. P-value of one-way anova, (**) P<0.001. PER activity was measured at 25°C by following the oxidation of 8 mM guaiacol (Fluka) at 470 nm in the presence of 2 mM H_2O_2 (Carlo Erba) in a phosphate buffer (200 mM, pH6.0).

***RSL4* Responsive Elements (RSL4-RE) and AUX Responsive Elements (Aux-RE) identification.** Meme from the MEME suite (2) was used to perform a motif search within five hundred base pairs upstream of genes regulated by RSL4 (downregulated in *rsl4-1* and upregulated in RSL4^{OE} line) (5). Those motifs showing a significant (evalue <1×10^{-10}) and present in more than 70 % of the sequences, where fed to TOMTOM (against the Jaspar core and *Arabidopsis* databases) to discard known motifs. As a result, a unique motif was obtained TN5-6CA[CT]G[TA]. By mean of FIMO, this putative motif was used to find single occurrences in promoter regions of the *Arabidopsis thaliana* genome (TAIR10, within 3000 bp of the transcription start site, with p<1×10^{-5}). We then searched for occurrences of the identified motif regular expression TN5-6CA[CT]G[TA] within 2000 bp upstream of *RBOH*, *PER* and *RSL4* genes. In a similar manner, we also searched for Aux-RE TGTCN[CG] and [GC]NGACA reported (6-7) in the upstream 1000 bp region of RSL4.

RSL4-PER co-expression analysis network. Co-expression networks for *RSL4* (cluster 172) were identified from AraNet (http://aranet.mpimp-golm.mpg.de/aranet) and trimmed to facilitate readability. Each co-expression of interest was confirmed independently using the expression angler tool from Botany Array Resource BAR (http://bar.utoronto.ca/ntools/cgi-bin/ntools_expression_angler.cgi) and ATTED-II (http://atted.jp). Only those genes that are connected with genes of interest are included. Co-expression values are based on *Pearson* correlation coefficients where r-value ranges from -1 for absolute negative correlation, 0 for no correlation and 1 for absolute positive correlation.

Construction of ARF and RSL4 transgenes. The *EXPA7* promoter (pE7):GFP construct in the modified binary vector, pCAMBIA1300-NOS (44), was used as the cloning vector to direct root hair-specific expression or to make GFP fusions. For root hair-specific expression constructs of *ARF*s, genomic *ARF* fragments were generated by PCR using the primer sets listed in **Table S4** and inserted into the pE7:GFP construct by replacing the GFP fragment. To construct pRSL4:RSL4-GFP, the *RSL4* promoter (pRSL4) region (-928~+63 bp relative to the predicted transcription initiation site) and the RSL4 coding region without the stop codon were generated by PCR using the primers listed in **Table S4** and Arabidopsis genomic DNA as template. pRSL4 and RSL4 fragments were sequentially inserted before the GFP gene of the pE7:GFP construct. For estradiol-inducible *pMDC7:ARF5-GFP* and *pMDC7:ARF7-GFP* constructs, *ARF5* and *ARF7* coding regions without their stop codon were generated by PCR using the primers listed in **Table S4** inserted before the *GFP* fragment of the pE7:GFP construct to make *ARF5,7,8-GFP* fusions. To transfer the *ARF-GFP* fragments to the pDONR207 vector, the *ARF5,7,8-GFP* regions were amplified by PCR using the primers for the site-specific recombination cloning system as listed in

Table S4. Each resulting amplified fragment was transferred to *pDONR207* using standard Lambda Integrase (Elpisbio, Korea). After confirmation of the inserts by nucleotide sequencing, the Lambda Integrase/Excisionase (Elpisbio, Korea) reaction was performed with the resulting *pDONR207-ARFs:GFP* plasmids and the binary vector *pMDC7*(8). To make the $_{pARF5}$:*GUS* reporter system, the amplified *GUS* fragment using the primers listed in **Supplementary Table S4** was inserted into the *pCAMBIA 1300-NOS* vector. The *ARF5* promoter region (-2071 to -1 from the start codon) was amplified using the primers listed in **Supplementary Table S4** and Arabidopsis genomic DNA as template and then inserted into the *pCAMBIA 1300-GUS:GFP-NOS* vector.

Chromatin ImmunoPrecipitation and PCR analysis. Chromatin immune-precipitation (ChIP) assay was performed as described previously (9-11). Seedlings grown for 10 days in the 0.5xMS medium were vacuum-infiltrated with 1% formaldehyde for cross-linking. For preparation of the ChIP analysis seedlings from estradiol-inducible $_{pMDC7}$:*ARF-GFP* transformants, as well as for $_{pRSL4}$:*RSL4-GFP* the seedlings were germinated for 4 days in 1 μM estradiol-containing medium (no induction in the case of pRSL4 line). After quenching the cross-linking by adding glycine, seedlings were ground in liquid nitrogen. Chromatin was isolated as described (12), resuspended in the nuclei lysis buffer (50 mM Tris-HCl pH8.0, 10 mM EDTA, 1% SDS), and sonicated to get 0.5-1.0 kb fragments. The chromatin solution was pre-cleared with the salmon sperm DNA/Protein-A agarose beads (Millipore, Germany) at 4℃ for 1 h and immune-precipitated with GFP antibody (MBL, Japan) for overnight. The immuno-complex was washed and eluted from the beads. Cross-linking was reversed by adding 5 M NaCl (final 200 mM) for 7 h at 65℃, and the sample was treated with proteinase K (final 40 ng μl^{-1}) to remove all the proteins. Antibody-untreated samples for estimation of input DNA also went through the same processes. Purification of DNA from the reverse crosslinked samples was done using the QIAquick PCR purification Kit (Qiagen, Germany). The quantitative PCR analyses were done using the primer sets listed in **Table S4**. The enrichment fold of each ChIP-PCR fragment was calculated first by normalizing the fragment amount against the input value and then by normalizing the value from transgenic plants against that from control plants.

Quantitative reverse transcriptase PCR (qRT-PCR). Total RNA was isolated from 10-d-old seedling roots (40 for each line) using the RNeasy Plant Mini Kit (Qiagen, Germany). cDNA was synthesized using TOPscript^{TM} RT DryMIX (dT18, Enzynomics, Korea). qRT-PCR analyses were performed using TOPrealTM qPCR 2x PreMIX (SYBR Green, Enzynomics, Korea) and Chromo4™ Four-Color Real-Time Detector (Bio-Rad, USA). Gene-specific signals were normalized relatively to *ACTIN7* (At5g09810) signals. Each qRT-PCR reaction was performed in triplicate, and each experiment was repeated three times using independent preparations of RNA. Primers used are as listed in **Table S4**.

Semiquantitative quantitative reverse transcriptase (RT-PCR). RNA was isolated from the roots with an RNA isolation kit (RNeasy, Qiagen, Hilden, Germany). For semiquantitative RT-

PCR, RNA was isolated from *Arabidopsis* roots. Reverse transcription of 1 mg of total RNA was performed with oligodT Primer. First strand synthesis was performed with a kit from Qiagen (Omniscript, Qiagen, Hilden, Germany). RT-PCR was conducted with the primer pairs given in **Table S4**. 10 days old roots were removed from plates growth in vertical position, rinsed 6 times with an excess of sterile water and were frozen in liquid nitrogen for RNA extraction. Semiquantitative analysis was performed after 27-32 PCR cycles: the products were analyzed on 2% agarose gels, stained with ethidium bromide, and visualized bands were quantified with the ImageJ 1.50b software. The mRNA levels for each cDNA probe were normalized with respect to *PPA2* (*AT1G69960*; serine/threonine protein phosphatase 2A) message levels.

Histochemical analysis and GUS assay. Seedlings of transgenic and wild type plants were incubated with GUS staining solution (100 mM $NaPO_4$ pH7.0, EDTA 10 mM, Triton X-100 0.1%, $K_3Fe(CN)_6$ 1 mM, X-Gluc 2 mM) 16 h at 37℃ and then de-stained in 70% ethanol. Whole roots were imaged using a Leica M205 FA Microscope.

ARFs expression in the root. Lines expressing ARF5, ARF7, ARF8 and ARF19 tagged with SV40 nuclear localization signals and 3 copies of GFP ($_{pARF}$::SV40-3xGFP) were used to track the expression of these ARFs in the root (19). In addition, $_{pARF5}$:GUS-GFP was used to study the ARF5 expression.
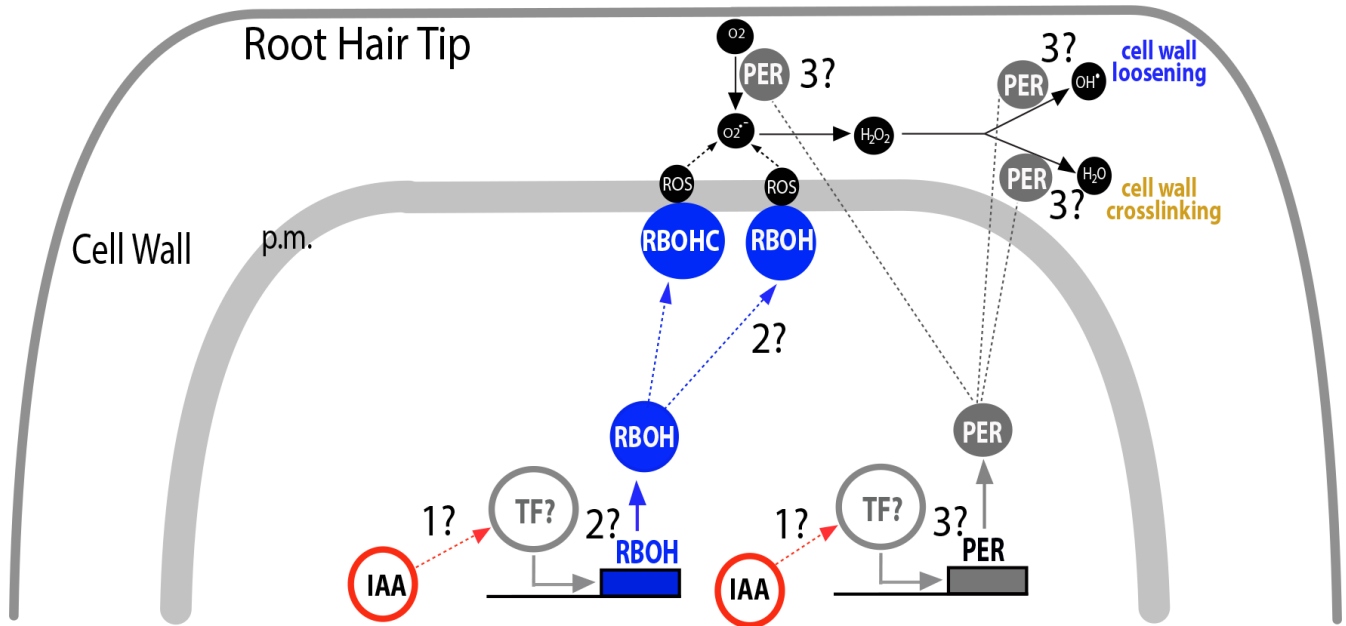
Figure S1. Question to be addressed on how auxin is linked to Reactive Oxygen Species (ROS) mediated root hair polar-growth in *Arabidopsis*. Current questions (denoted as 1?-3?) to be addressed in the current study. In growing root hair cells auxin enhances root hair growth possibly by activating a putative/s transcription factor/s (TF) (*question 1*?). Auxin triggers the production of apoplastic ROS by regulating the expression of RBOHC, and possibly others unknown RBOHs (*question 2*?) as well as by unknown PERs (*question 3*?). Apoplastic ROS trigger cell wall loosening as well as cell wall crosslinking reactions mediated by putative Class-III peroxidases (PERs). Reactive Oxygen Species (ROS): hydroxyl radical ($^{\bullet}OH$); superoxide ion ($O_2^{\bullet -}$), hydrogen peroxide (H_2O_2); singlet oxygen (O_2).
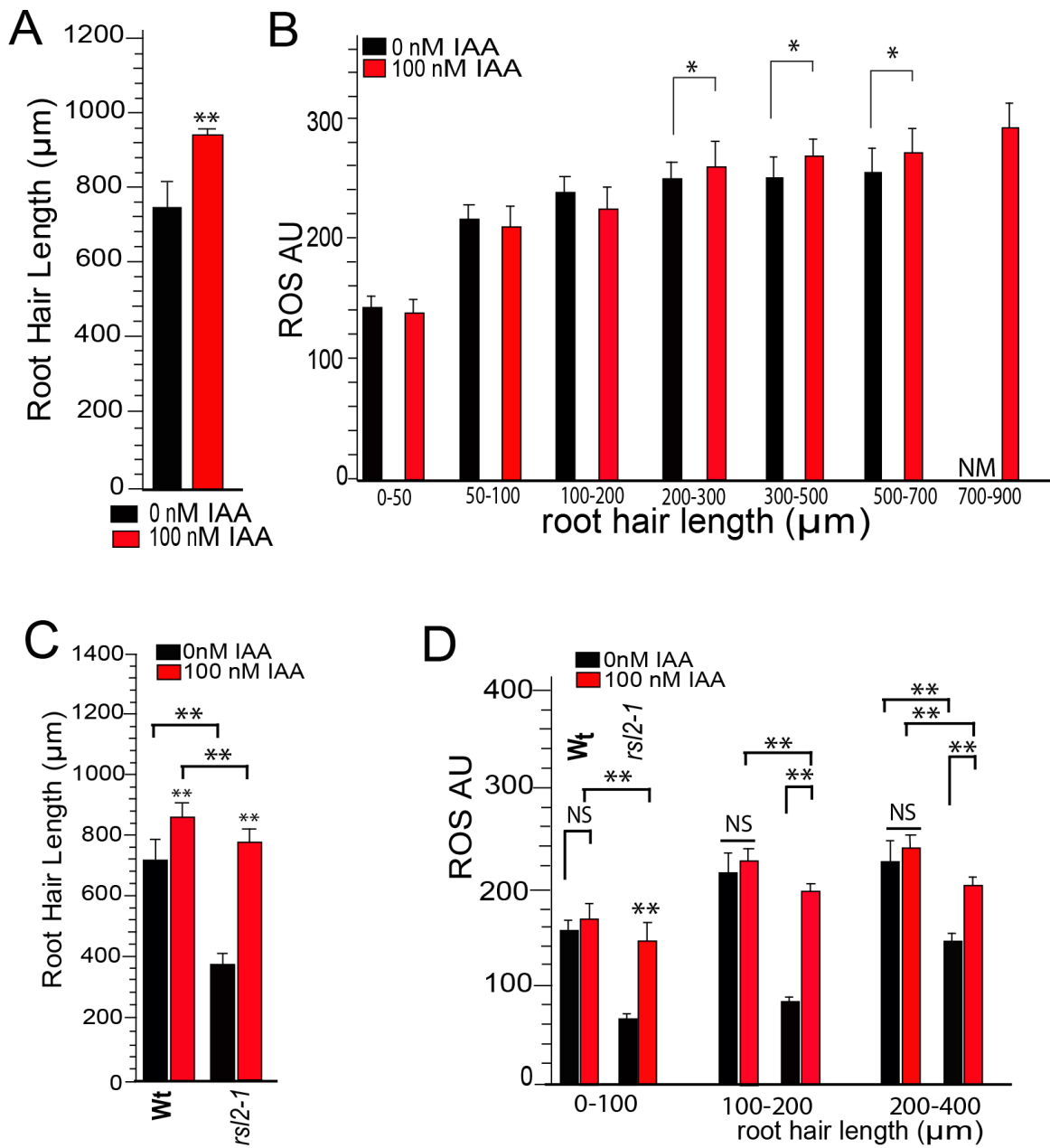
Figure S2. ROS-production linked to polar-growth is modulated by auxin. A, Quantitative analysis of root hair length (mean ± SD) in Wt Col-0 treated with treated with auxin (100 nM IAA). **B**, ROS signal analysis generated by ROS-mediated oxidation of H_2DCF-DA in several developmental stages of Wt Col-0 root hairs under auxin treatment (mean ± SD). AU= arbitrary units. *P*-value of one-way anova, (*) P<0.05, (**) P<0.001. NM= Not measured. Auxin-treated roots are compared to non-treated ones. **C,** Root hair length (mean ± SD) in Wt Col-0 and *rsl2-1* treated with 100nM IAA. **D,** Effect of auxin (100nM IAA, indole 3-acetic acid) mediated by RSL2 on ROS production. ROS signal analysis with IAA treatment of Wt Col-0 and *rsl2-1* mutant in the early stages of root hair development.
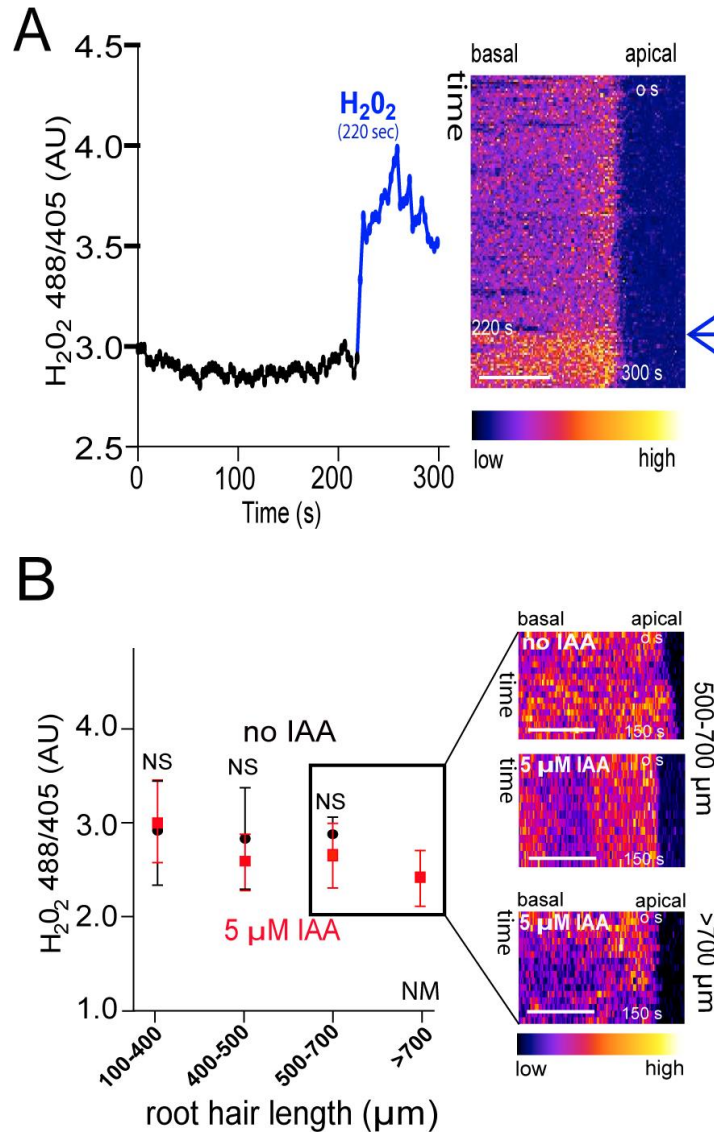
Figure S3. $_{cyt}H_2O_2$ levels in response to auxin-treatments in root hair tips by HyPer imaging. **A**, Short term H_2O_2 treatment monitored with HyPer. H_2O_2 was added at 220 sec of initial time recording (blue arrow). On the right, kymograph of HyPer expressing root hair. **B**, HyPer imaging of $_{cyt}H_2O_2$ signal along different developmental stages of Col-0 root hairs grown with and without 5 μM IAA. Scale Bar = 5 μm. On the right, kymographs resulting of this analysis for root hairs at late developmental stages of 500->700 μm in length. Scale bar = 5 μm. NS= not significant difference. Non-IAA treated Wt Col-0 roots did not develop root hairs longer than 700 μm in cell length. NM= not measured.
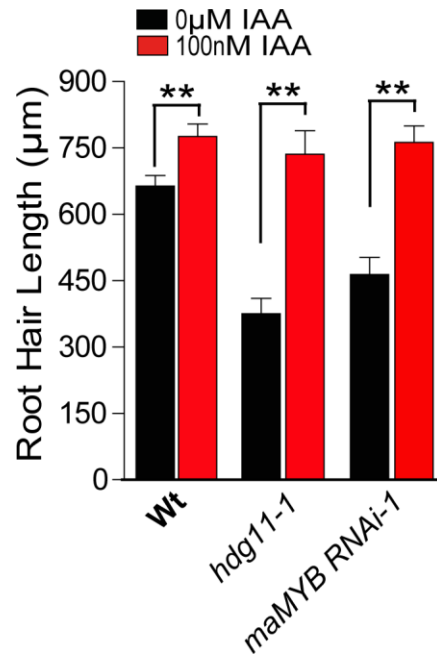
**Figure S4. Auxin treatment in *hdg11-1* and *maMYB* mutants.** Auxin-treatment (100 nM IAA) of TF *hdg11* and *MaMYB* RNAi-1 (silenced line 1) mutants restores Wt levels of root hair growth. Non-treated *hdg11* and *MaMYB RNAi-1* present a clear short root hair phenotype in comparison to Wt. *P*-value of one-way anova, (**) P<0.001 (n roots= 30). Comparisons between treatments are indicated (mean ± SD).
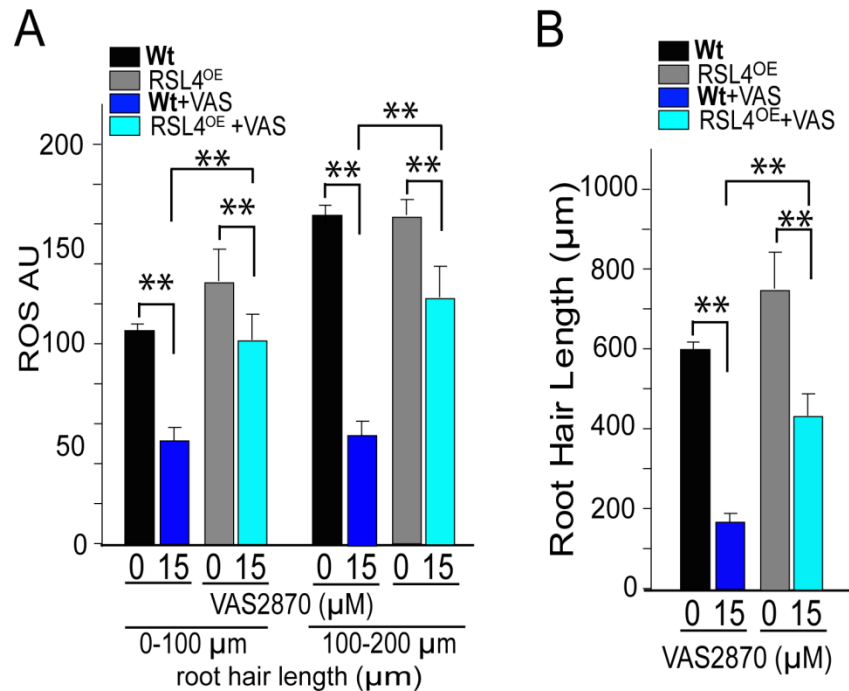
Figure S5. RSL4^{OE} line is less sensitive to ROS inhibition. A, ROS signal analysis of Wt Col-0 and RSL4^{OE} (RSL4 overexpressing line) when treated with 15 µM of RBOH inhibitor VAS2870 (VAS) in the early stages of root hair development (mean ± SD). *P*-value of one-way anova, (**) P<0.001. Comparisons are made on ROS levels between control/IAA treated within the same genotype. **B**, Quantitative analysis of root hair length (mean ± SD, n roots= 30) in Wt Col-0 and RSL4^{OE} treated with 15 µM of RBOH inhibitor VAS2870. *P*-value of one-way anova, (**) P<0.001. Comparisons are made on root hair length between different treatments in the same root hair specific developmental stage.

A

ARF5   ARF7   ARF8   ARF19

B

pARF::SV40-3xGFP

ARF5 EZ   ARF7 RH   ARF8 EZ

pARF5::GUS-GFP   pARF19::SV40-3xGFP

ARF5 MZ   ARF7 MZ   ARF8 MZ

C

ARF5   ARF7   ARF8

Relative expression level

Cont   P7:ARF5^OE   Cont   P7:ARF7^OE   Cont   P7:ARF8^OE

D

Cont   P7:ARF5^OE   P7:ARF7^OE   P7:ARF8^OE

E

P7:GFP
P7:ARF^OE

ROS AU

root hair length (μm)

0-200   200-400   400-600   600-700   700-900
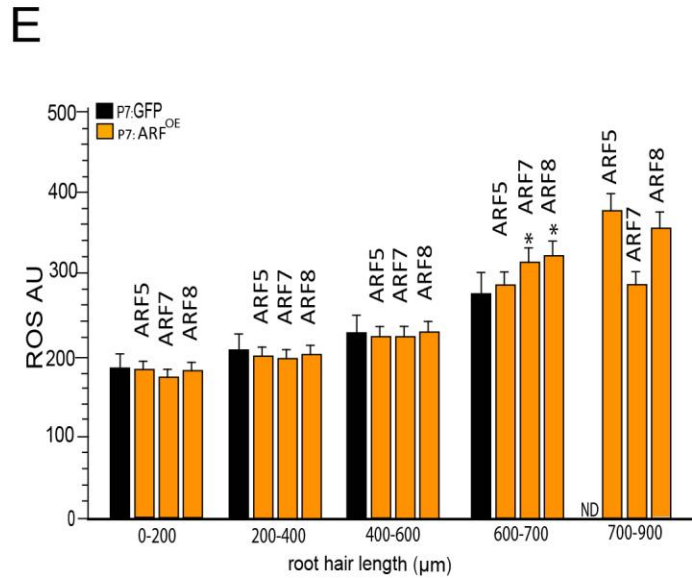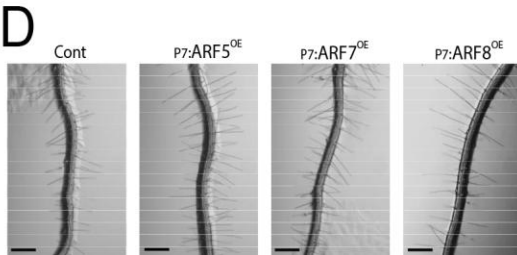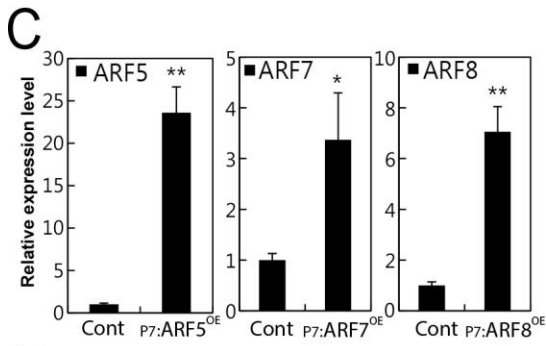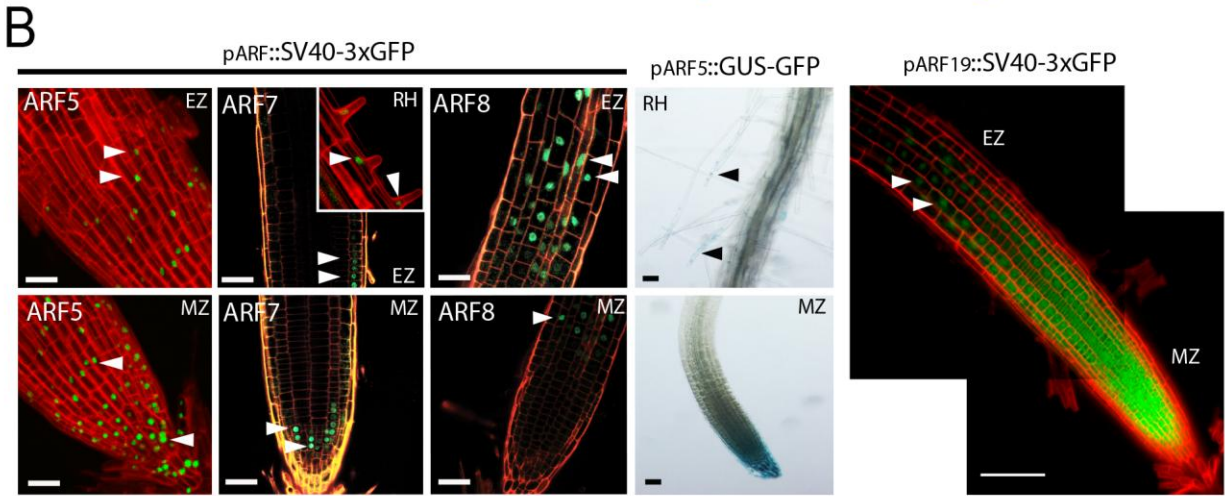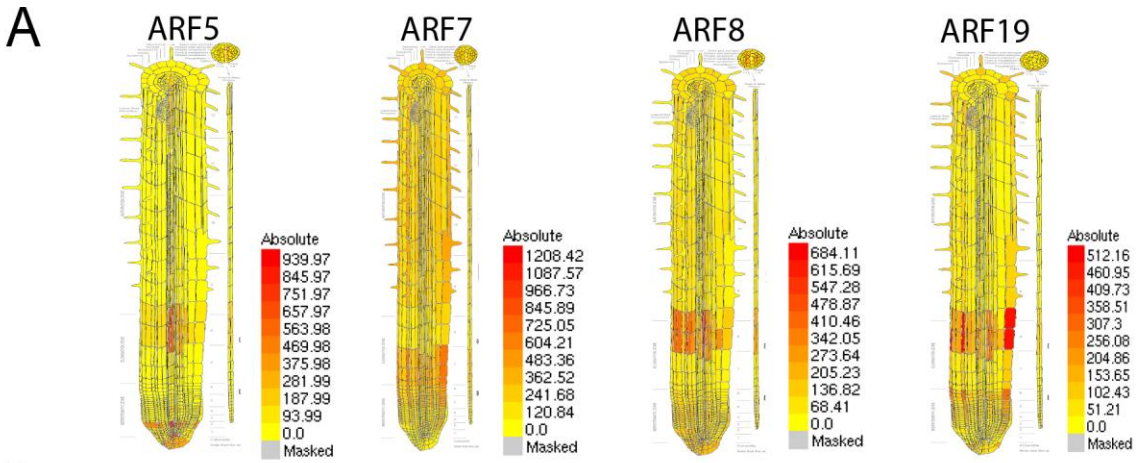
Figure S6. Main ARFs responsible for auxin-mediated RSL4 expression and root hair growth. A, Root expression patterns of ARF5,7,8,19 based on Arabidopsis eFP Browser. These ARFs are the most abundant in epidermis cells. **B**, Expression pattern of ARF5, ARF7, ARF8 and ARF19 in the meristematic root zone (MZ), in the elongation root zone (EZ) and in the root hair cells (RH). *pARF::SV40-3xGFP* reporters for ARF5,7,8,19 as well as *pARF5::GUS-GFP* reporter were analyzed. Expression of *pARF5:GUS* was shown in the root tip and root hairs. Arrowheads indicate the GFP expression and arrows GUS expression. Scale bar= 100 µm. **C,** Transcript levels of ARF mRNAs in $_{P7:}$ARF^{OE} (ARF overexpressing lines under the control of EXPANSIN 7 promoter (P7). Error bars indicate ±SD. Results were from two biological samples for qRT-PCR. The values are relative to the Cont (Control) value and significantly different (**, $P < 0.001$; *, $P<0.01$; t-test) from the Cont value. **D,** Root hair phenotypes of control (Cont, $_{pE7:}$GFP) and ARF-overexpression transformants (ARF^{OE}, $_{pE7:}$ARF5,7,8). n roots= 30. Scale bar = 400 µm. **E,** ROS signal analysis generated by ROS-mediated oxidation of H_2DCF-DA in several root hair developmental stages of $_{P7:}$GFP (control) and ARF-overexpression lines (ARF^{OE}, $_{pE7:}$ARF5,7,8) (mean ± SD). AU= arbitrary units. *P*-value of one-way anova, (*) $P<0.01$.
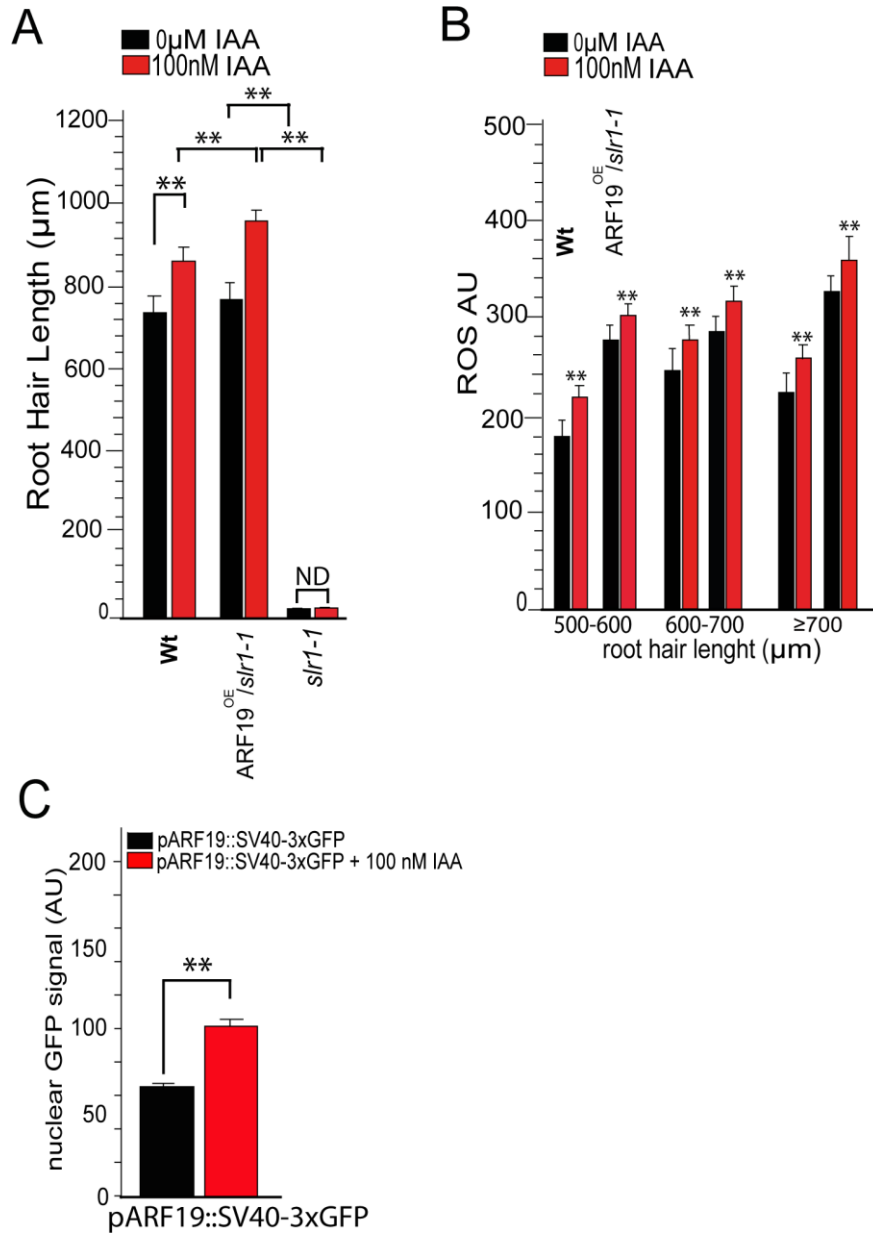
Figure S7. Auxin-responsive ARF19 is involved in ROS-linked root hair growth. A, Quantitative analysis of root hair length (mean ± SD) in Wt Col-0, *srl1-1*(IAA/Aux14), and *srlr1-1*/ARF19[OE] non-treated and treated with IAA (100 nM IAA in 0.5X MS). *P*-value of one-way anova, (**) P<0.001. **B**, ROS signal analysis of Wt Col-0 and *sr1-1* (IAA/Aux14)/ARF19[OE] (mean ± SD). *P*-value of one-way anova, (**) P<0.001. ND= not detected. **C**, Quantitative analysis of ARF19 nuclear expression in roots treated with IAA (100 nM IAA IAA) (mean ± SD). *P*-value of one-way anova, (**) P<0.001. The transgenic line express ARF19 under its endogenous promoter tagged with SV40 nuclear localization signals plus 3 copies of GFP (pARF19:SV40-3xGFP).
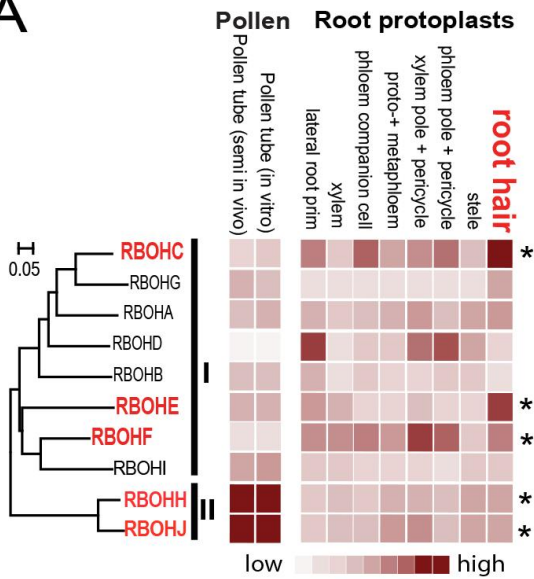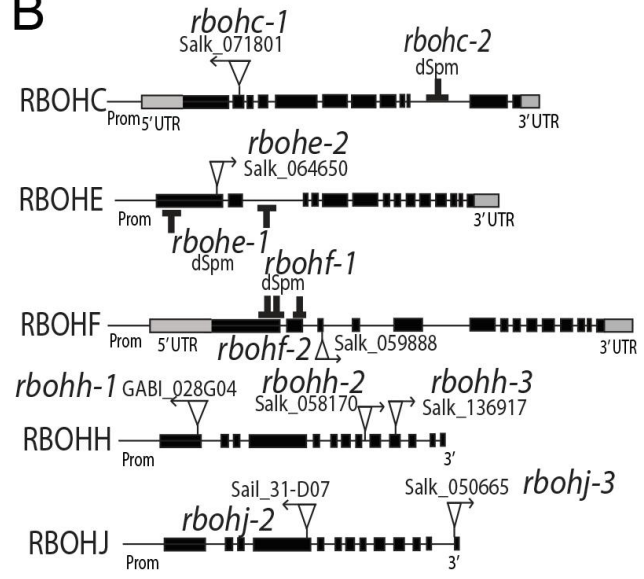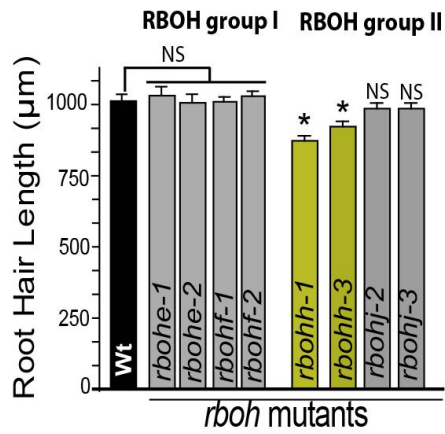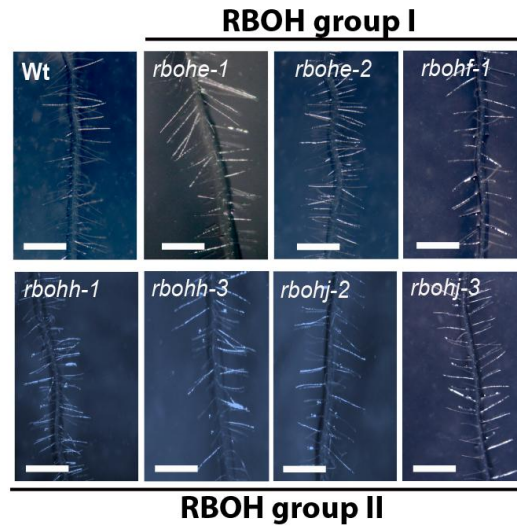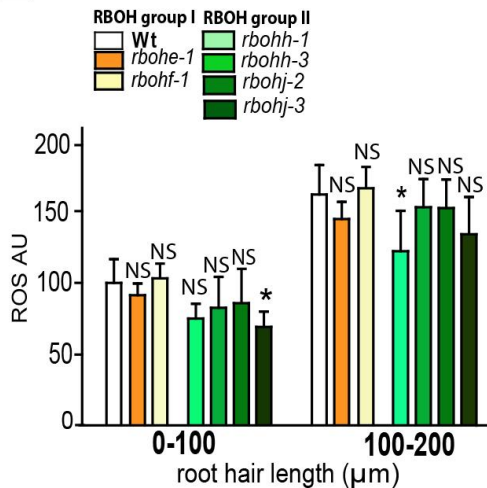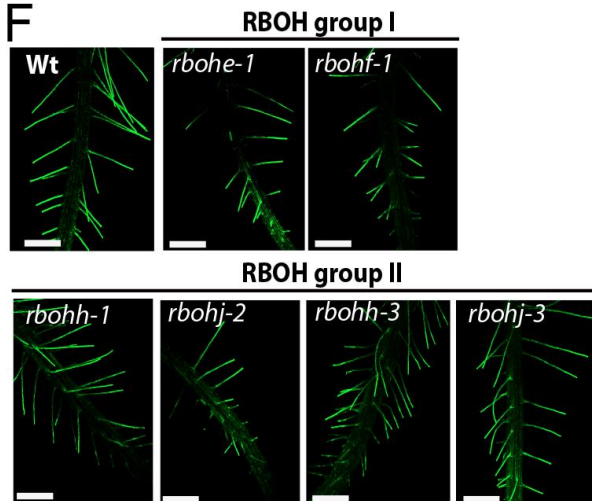
Figure S8. RBOHH and RBOHJ alone poorly contribute to ROS-mediated root hair cell expansion in *Arabidopsis*. A, Multiple alignments of *Arabidopsis* RBOH proteins are shown as a tree using the protein sequence parsimony method. The tree was then combined with the relative gene expression of *Arabidopsis RBOH* family members in several chosen plant tissues (roots protoplast and pollen) according to the Genevestigator microarray database using the Meta-Profile Analysis tool, Anatomy Profile. The expression level (in red color) is relative to each gene maximum expression level. (*) indicates root hair high expression at transcriptional level. **B**, Root hair-expressed *RBOH* gene structure and positions of the corresponding T-DNA (GABI, SAIL and Salk lines) and transposon (dspm) insertions in the mutants used in this study. The orientation of the left border sequence of the respective T-DNAs is represented by black arrows. **C**, Quantitative analysis of root hair length (mean ± SD) in single and multiple *rboh* mutants. NS= not significant difference. *P*-value of one-way anova, (*) P<0.01. **D**, Root hair phenotype in Wt Col-0 and single *rbohc* mutants. Scale bar = 600 μm. **E-F,** ROS signal analysis generated by ROS oxidation of the H_2DCF-DA probe in early stages of root hair development of single *rboh* mutants (mean ± SD). **e**, Comparisons are made on ROS levels between Wt Col-0 and each *rboh* mutant genotype unless otherwise indicated. AU= fluorescent arbitrary units. *P*-value of one-way anova, (*) P<0.01. NS= not significant difference. **F**, ROS H_2DCF-DA staining in roots of Wt Col-0 and single *rboh* mutants. Scale bar = 600 μm.

A

B

C

D

E

F

initial growth → early cell elongation → later cell elongation

RBOHC   RBOHC + RBOHH,J   RBOHH,J

ROS
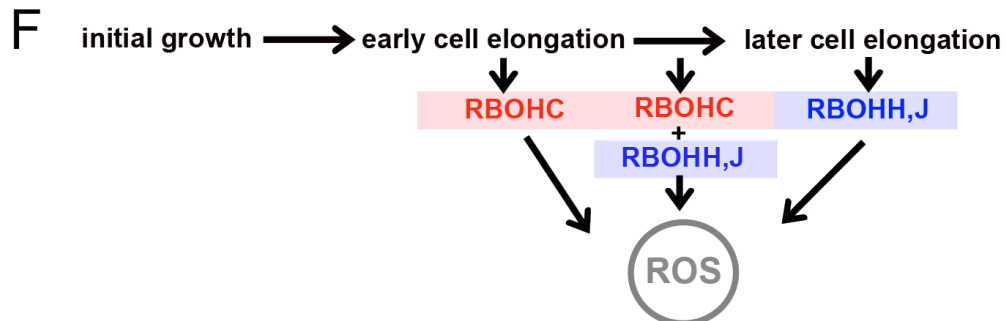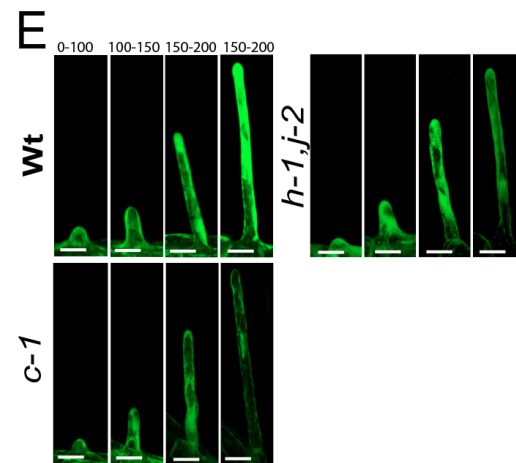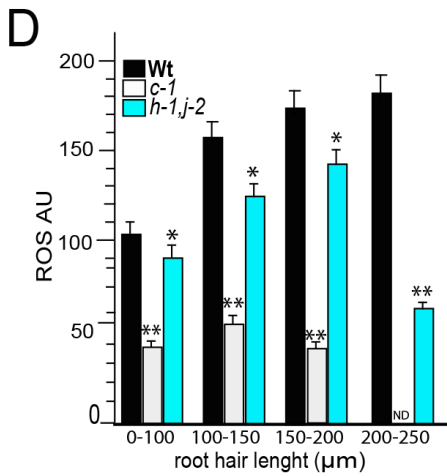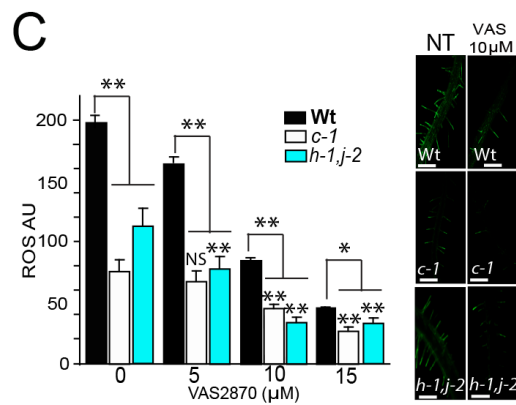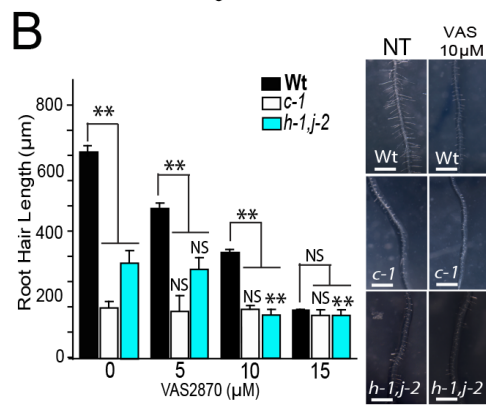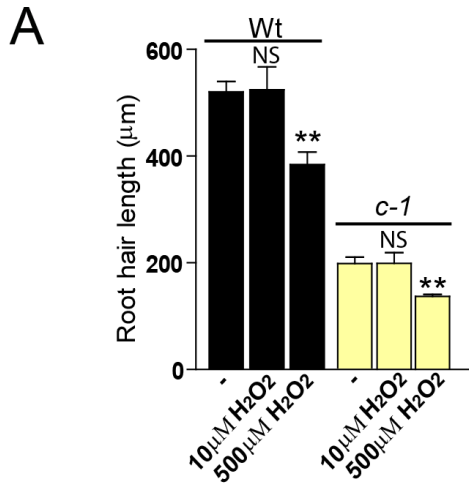
Figure S9. RBOHC,H,J promote ROS-mediated root hair polar-growth but not required at initial developmental stages. A, exogenous H_2O_2 application fails to rescue the root hair growth defect in the ROS-deficient *rbohc-1* mutant (mean $\pm$ SD). *P*-value of one-way anova, (*) P<0.01. NS= not significant different. **B**, ROS is not required for initial development of root hairs. Quantitative analysis of root hair length (mean $\pm$ SD., n roots= 30) in Wt Col-0 and *rbohc* mutant non-treated and treated with up to 10 μM of VAS2870 RBOH inhibitor. Inhibitory Concentration 50 (IC_{50}) of VAS for root hair growth was 7.5 μM. Only root hairs of 0-100 μm were included. NS= not significant difference. *P*-value of one-way anova, (**) P<0.001, (*) P<0.01. Comparisons are made within each genotype under different inhibitor concentrations unless otherwise indicated. On the right, root hair phenotype in Wt Col-0 and *rbohc* non-treated and treated with up to 10 μM of VAS2870. Scale bar = 600 μm. **C**, Residual ROS signal in *rbohc-1* and *rbohh rbohj* mutants. Treatment with up to 10 μM of VAS2870 abolished ~90% ROS (mean $\pm$ SD). IC_{50} of VAS for ROS was 7.0 μM. AU= arbitrary units. *P*-value of one-way anova, (**) P<0.001. Comparisons are made within each genotype ROS levels and under different inhibitor concentrations. On the bottom, ROS signal suppression in Wt Col-0 and *rboh* mutants treated with 10 μM of VAS2870 RBOH inhibitor. Scale bar = 300 μm. **D**, ROS signal analysis of Wt Col-0 and *rboh* mutants in the early stages of root hair development (mean $\pm$ SD). Only root hairs of 0-100 μm and 100-200 μm were included. NS= not significant difference. *P*-value of one-way anova, (**) P<0.001, (*) P<0.01. NS= not significant different. Comparisons are made on root hair length between genotypes at root hair specific developmental stages. **E**, ROS H_2DCF-DA signal in growing root hairs (0-200 μm in length). Scale bar = 30 μm. **F**, Proposed sequence of events of ROS-production by RBOHC and RBOHH,J linked to polar root hair growth.
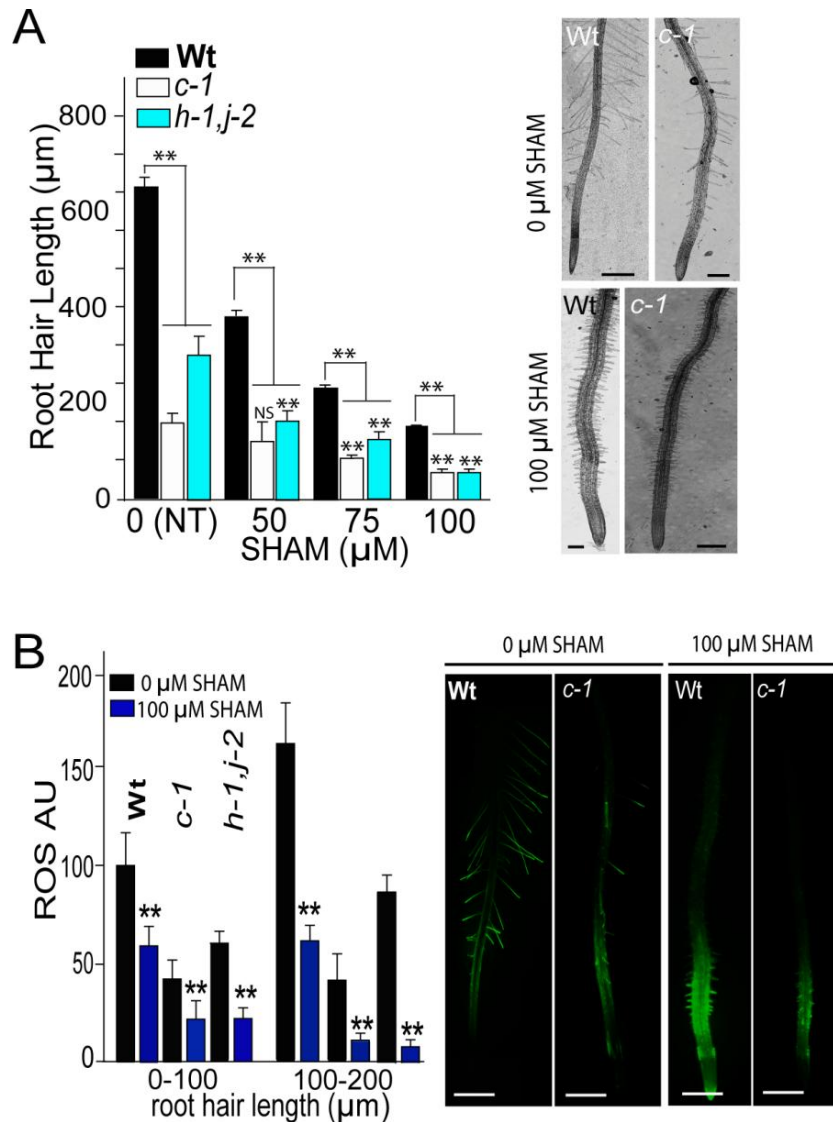
Figure S10. PERs impact on ROS-homeostasis and root hair polar-growth. A, Quantitative analysis of root hair length (mean ± SD) in single and multiple *rboh* mutants (*c-1* and *h-1,j-2*) treated with up to 100 μM SHAM (PER inhibitor). Comparisons are made within each genotype under different inhibitor concentrations unless otherwise indicated. NS= not significant difference. *P*-value of one-way anova, (**) P<0.001. Scale bar = 300 μm. **B**, ROS signal analysis generated by ROS oxidation of H₂DCF-DA in early stages of root hair development in single and multiple *rboh* mutants (*c-1* and *h-1,j-2*) treated with SHAM(mean ± SD). AU= fluorescent arbitrary units. *P*-value of one-way anova, (**) P<0.001. On the right, ROS H₂DCF-DA staining in roots of Wt and *rbohc-1* mutant. Scale bar = 300 μm for Wt and *c-1* (0 μM SHAM). Scale bar = 200 μm for Wt and *c-1* (100 μM SHAM).
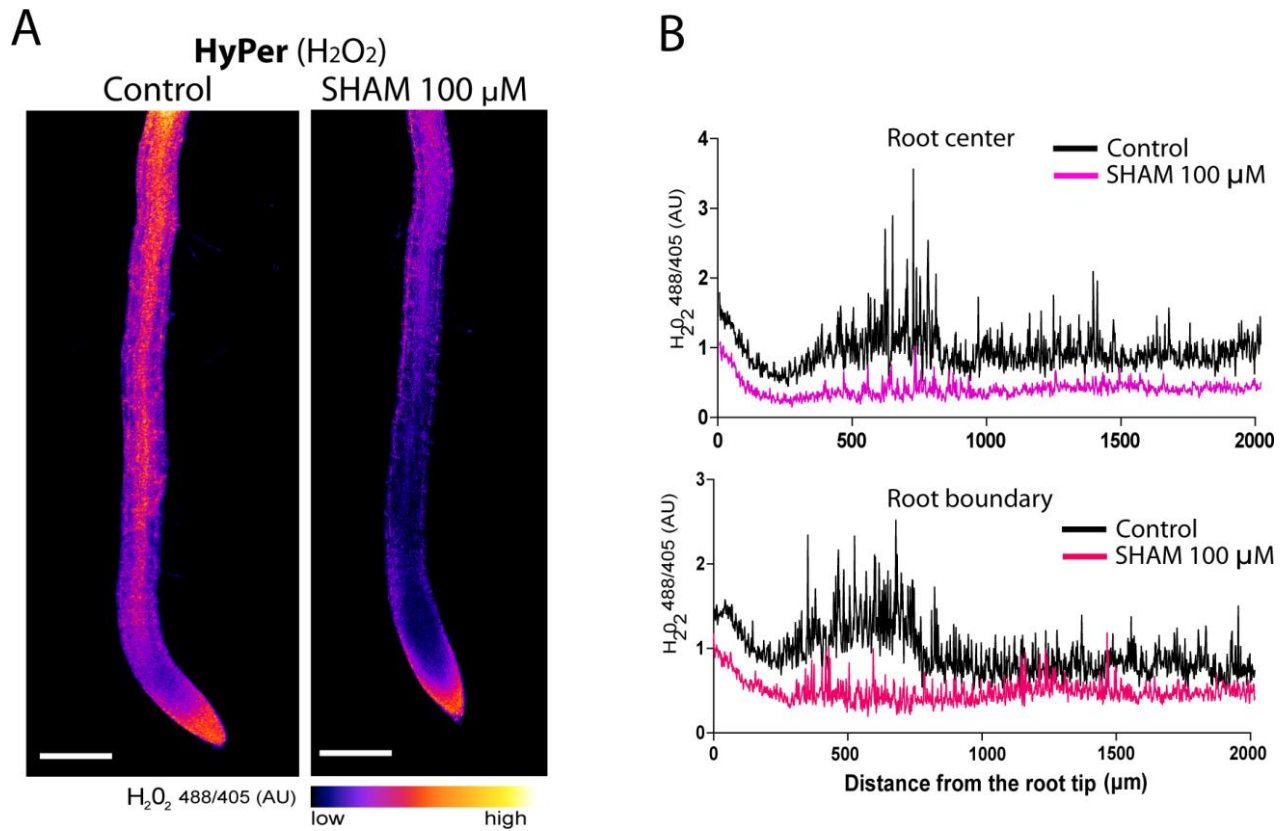
Figure S11. Secreted type-III PER contribution to $_{cyt}H_2O_2$ signal in the roots. A, HyPer imaging of $_{cyt}H_2O_2$ signal in the whole roots of Wt Col-0 without and with SHAM. Scale Bar = 400 μm. AU= Arbitrary Units based on the ratio between 488/405nm. Scale bar = 600 μm. **B**, Quantification of HyPer signal in the root center (top) and root boundary (bottom).
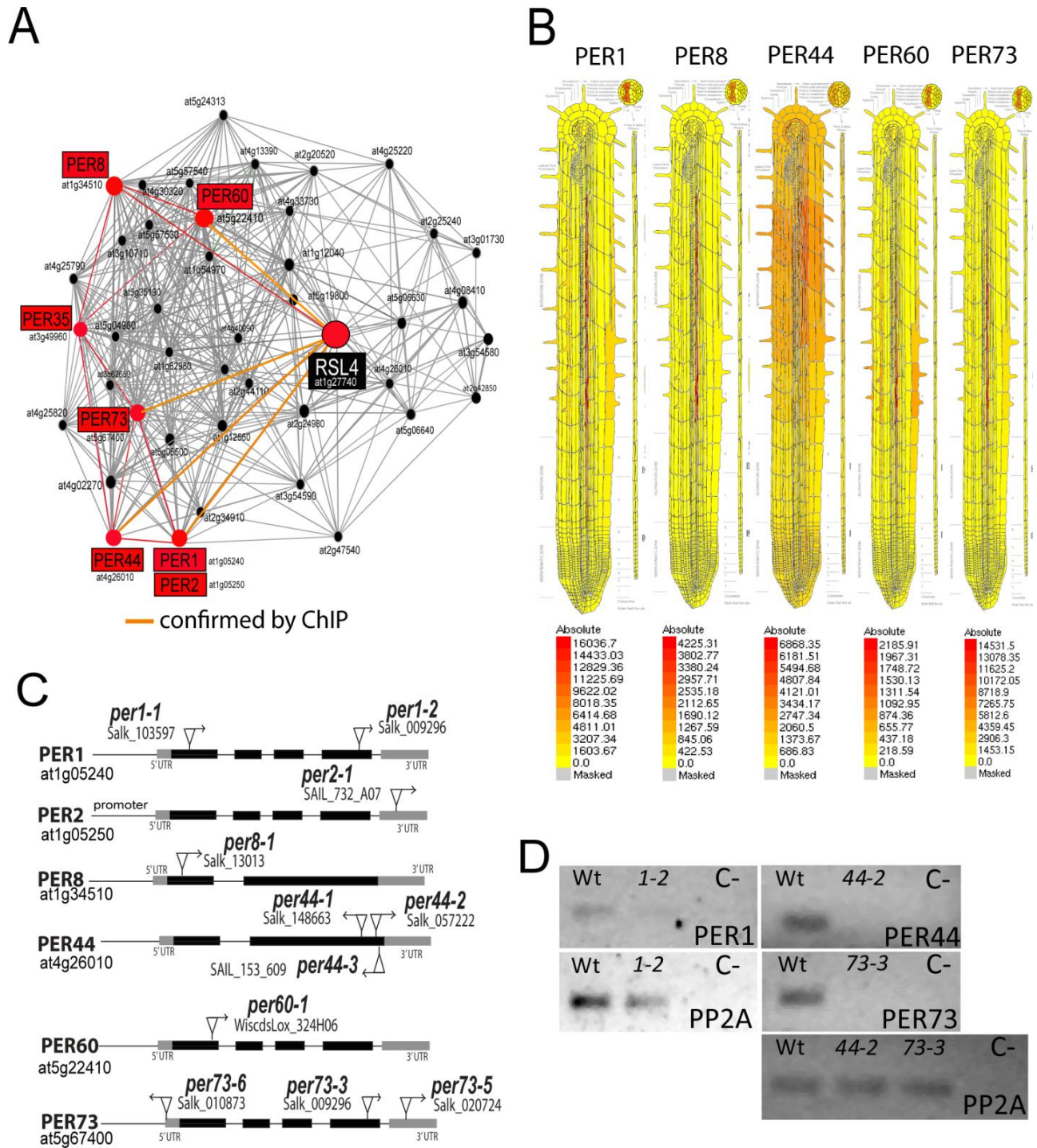
Figure S12. Identification of root hair specific PERs. A, Several *PERs* are highly co-expressed with *RSL4*. Co-expression values are based on *Pearson* correlation coefficients where r-value range from -1 for absolute negative correlation, 0 for no correlation and 1 for absolute positive correlation. Only high positive values were considered (cut off =0.7). Yellow lines indicate RSL4

binding on PER promoters identified by chromatin immunoprecipitation (ChIP) assay (see **Figure 3d**). **B**, Root expression patterns of *PER1, 8, 35, 60, 73* based on Arabidopsis eFP Browser. These *PERs* are abundant in root hair protoplast cells. **C**, Gene structure and T-DNA mutants isolated for root hair specific *PERs* associated with *RSL4* regulation. **D**, RT-PCR of *per1-2, 44-2*, and *per73-3* mutants. *PP2A* (AT1G69960; serine/threonine protein phosphatase 2A) was used as housekeeping gene. C- = negative control.
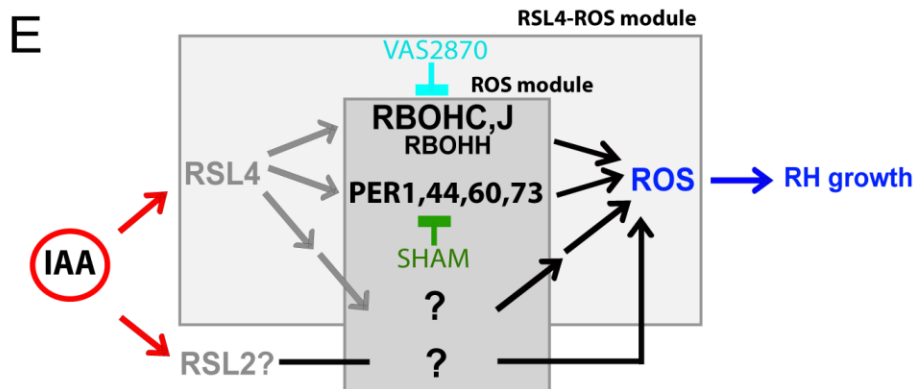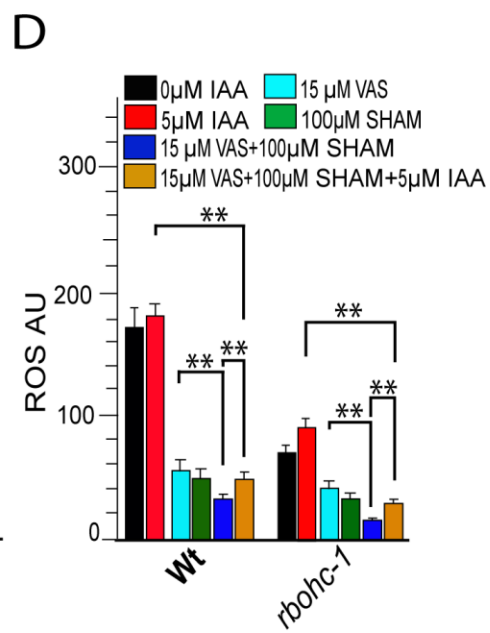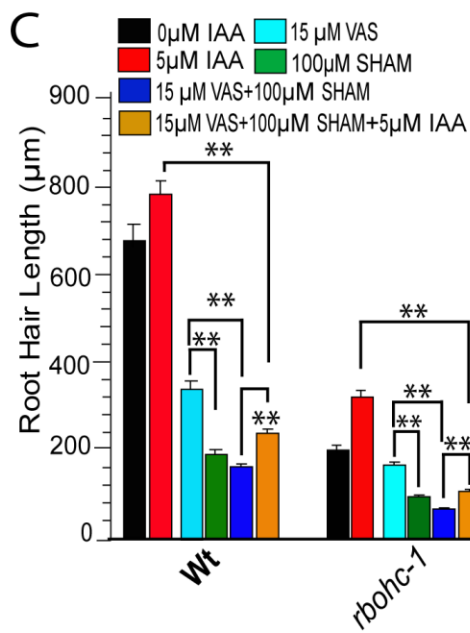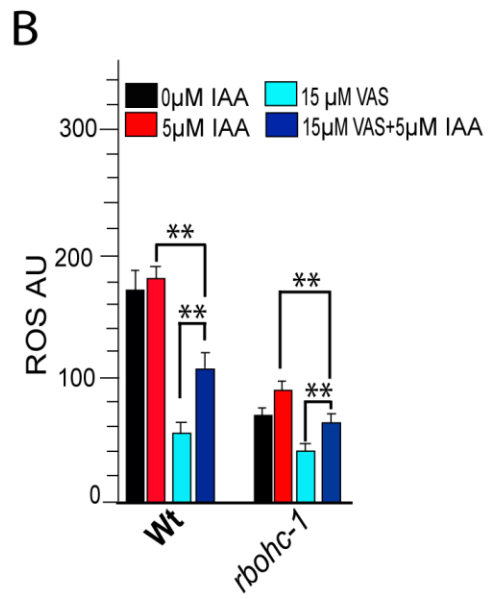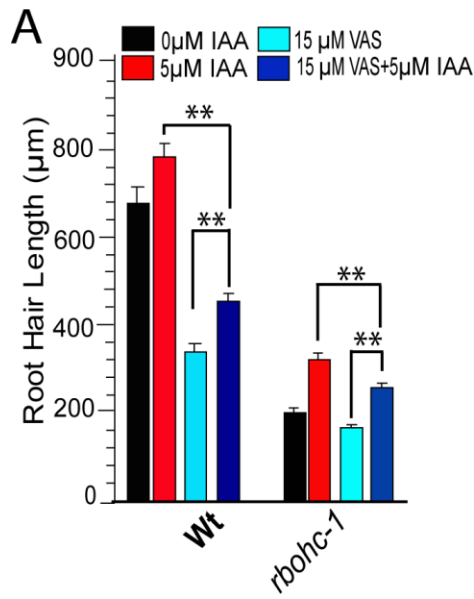
Figure S13. Auxin requires RBOH- and PER-related ROS to trigger root hair polar-growth.
A, Quantitative analysis of root hair length (mean ± SD) in Wt Col-0 and in *rbohc-1* mutant treated with IAA (5 μM IAA), VAS2870 15 μM, and IAA+VAS. NS= not significant difference. *P*-value of one-way anova, (**) P<0.001, (*) P<0.01 (n roots= 30). Comparisons are made on root hair length between different treatments in the same root hair specific developmental stage. **B**, Quantitative analysis of ROS signals in *rbohc-1* mutant treated with IAA (5 μM IAA), VAS2870 (VAS 15 μM) and IAA+VAS (mean ± SD). NS= not significant difference. *P*-value of one-way anova, (**) P<0.001, (*) P<0.01. Comparisons are made on ROS levels between control/IAA treatments in the same root hair specific developmental stage for each genotype. Root hairs of 0-200 μm in length were analyzed. **C**, Quantitative analysis of root hair length (mean ± SD, n roots= 30) in Wt Col-0 and in *rbohc-1* mutant treated with IAA (5 μM IAA), VAS2870 (VAS 15 μM), SHAM (100 μM), VAS + SHAM, and VAS + SHAM + IAA. NS= not significant difference. *P*-value of one-way anova, (**) P<0.001, (*) P<0.01. Comparisons are made on root hair length between different treatments in the same root hair specific developmental stage. **D**, Quantitative analysis of ROS signals in *rbohc-1* mutant treated with IAA (5 μM IAA), VAS2870 (VAS15 μM), SHAM (100 μM), VAS2870 + SHAM, and VAS + SHAM + IAA(mean ± SD). *P*-value of one-way anova, (**) P<0.001, (*) P<0.01. Comparisons are made on ROS levels between control/IAA treatments in the same root hair specific developmental stage for each genotype. Root hairs of 0-200 μm in length were analyzed. **E**, Proposed sequence of events from IAA signal to root hair (RH) growth sustained by a RSL4-RBOHs+PERs dependent pathways and a putative RSL4-independent pathway possibly mediated by RSL2. TF=Transcription Factor.
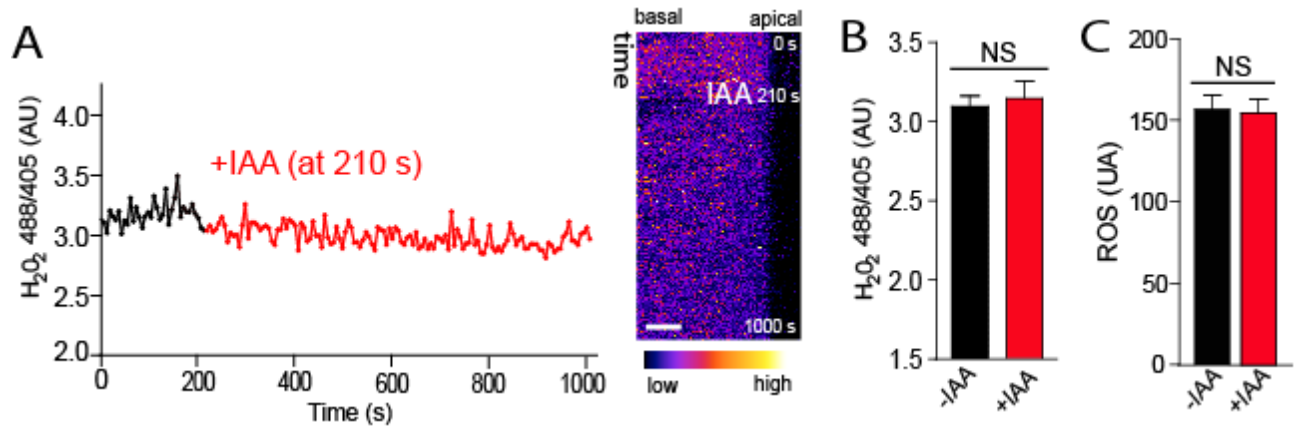
Figure S14. *In situ* auxin treatment. **A**, $_{cyt}H_2O_2$ levels in non-treated and then IAA-treated Wt Col-0 root hairs expressing HyPer sensor. $_{cyt}H_2O_2$ levels are based on the 488/405 nm ratio of HyPer at the root hair tip over 1000 seconds (s). On the right, selected kymographs. Scale bar = 5 μm. We have included one representative assay (n=5). **B**, Average and S.E.M signal 488/405 nm ratio of HyPer at the root hair tip (n=5). *P*-value of one-way ANOVA, NS= not significant difference. **C**, $_{cyt}$ROS levels quantified with the dye H_2DCF-DA in non-treated and then IAA-treated (100 nM) for Wt Col-0 root hairs of 0-100 μm in cell length (mean ± SD) . *P*-value of one-way ANOVA, NS= not significant difference.

Supplementary Table S1. RSLs, NADPH oxidases (RBOH) and secreted type-III Peroxidase (PER) mutant lines used in this study. All are in Col-0 background.

Name	Locus	Mutant name	Mutant code	References
			RSLs	
RSL2	*At3g33880*	*rsl2-1*	SAIL line 514C04	[5]
RSL4	*At1g27740*	*rsl4-1*	GT_5_105706	[5]
			RBOHs	
RBOHC	*At5g51060*	*rbohc-1*	Salk_071801	[13]
		rbohc-2	Transposable line (dspm)	[14-15]
RBOHE	*At1g19230*	*rbohe-1*	Transposable line (dspm)	[14-15]
		rbohe-2	Salk_064850	[15]
RBOHF	*At1g64060*	*rbohf-1*	Transposable line (dspm)	[13-14]
		rbohf-2	Salk_059888	[15]
		rbohf-3	Salk_034674C	[16]
RBOHH	*At5g60010*	*rbohh-1*	Gabi_028G04	[17-18]
		rbohh-3	Salk_136917	[17 -18]
RBOHJ	*At3g45810*	*rbohj-2*	Sail_31D07	[17-18]
		rbohj-3	Salk_050665	[17-18]
			PERs	
PER1	*At1g05240*	*per1-1*	sail_732_A07	This study
PER2	*At1g05250*	*per2-1*	salk_103597	This study
		per2-2	salk_009296	This study
PER8	*At1g34510*	*per8-1*	salk_130310C	This study
PER35	*At3g49960*	*per35-1*	salk_129866C	This study
PER44	*At4g26010*	*per44-1*	salk_148663C	This study
		per44-2	salk_057222C	This study
		per44-3	sail_153_609	This study
PER60	*At5g22410*	*per60-1*	WISCDSLOX324H06	This study
PER73	*At5g67400*	*per73-3*	salk_009296	This study
		per73-4	salk_020724	This study
		per73-5	salk_010873	This study

Supplementary Table S2. Aux-RE element in the upstream regulatory region of RSL4.

Position from start codon	Sequence	Direction
-863	GGTCTT	Reverse
-584	GGTCTC	Reverse
-575	TGTCCG	Reverse
-313	TGTCGT	Forward
-288	TGTCGA	Forward
-285	GGTCGA	Reverse
-209	TGTCGT	Reverse
-117	TGTCTC	Forward

Supplementary Table S3. Root Hair *cis*-Element (RHE) in the upstream regulatory regions of *RBOHs* (*RBOHC,H,J*) and *PERs* (*PER1,44,60,73*).

Gene	Position from start codon	Sequence	Direction
RBOHC *At5g51060*	-1410	CAAGTCCG-ACCACGTC	Forward
	-330	CATGTGAA-TTCACGAG	Forward
RBOHH *At5g60010*	-739	AGAGTGGC-GGCACGTG	Forward
	-803	CCTGTCTTCGTCACGTG	Reverse
	-809	GGGTTCGGTGGCACGTG	Forward
	-920	TTCTTGGCTGCCACGGT	Forward
RBOHJ *At3g45810*	-851	AAATTAGT-TCCACGAC	Reverse
PER1 *At1g05240*	-461	TTTGTGGAATCCACGTT	Reverse
	-1501	TAGCTTAATTGCACGTT	Reverse
PER44 *At4g26010*	-267	AGAATGAT-TCCACGCG	Reverse
PER60 *At5g22410*	-113	TCCATGAA-CGCACGTT	Forward
	-468	TTAGTAGTATCCACGTT	Forward
	-518	ATGATTTT-TGCACGTT	Forward
PER73 *At5g67400*	-199	AACTTGGA-GCCACGTT	Reverse
	-521	TTTTTGCTCTGCACGAA	Forward

Supplementary Table S4. Primer List.

Purpose	Name	Sequence (5' to 3')
ARF5	A5PacI-F	AACATTAATTAATCTCTCTGTATGATGGCTTC
	A5SgsI_R	TACAGGCGCGCCGTTTCTCCTCTACCAGTTGG
	A5SgsI_R(nonstop)	TTTGGCGCGCCATGAAACAGAAGTCTTAAG
ARF7	A7KpnI_F	TTATGGTACCGAGAAAGTAAAGTTGAGTGATCATG
	A7AvrII_R	TTATCCTAGGTGTGAGAGAACTCTTCTGC
	A7MluI_R(nonstop)	TATAACGCGTGACCGGTTAAACGAAGTGGCTGAG
ARF8	A8PacI_F	AAGTTTAATTAAACATGAAGCTGTCAACATCT
	A8SgsI_R	GAATGGCGCGCCAAGATGAGTGGAAACGA
pRSL4 & RSL4	ProR4HindIII-F	GGAAGCTTCAAGTATATAACAAAAGAATG
	ProR4BamHI-R	ACGTGGATCCCTCTAACTGATCAAC
	R4XmaI_F	TCAGCCCGGGCGATGGACGTTTTTGTTGAT
	R4AvrII_R	TAACTTGTAAGTCCTCCTAGGCATAAGCCGA
Site-specific recombination cloning for pMDC7-ARFs-GFP	attB1-ARF5-1F	GGGGACAAGTTTGTACAAAAAAGCAGGCTGTATGATGGCTTCATTGTCT
	attB1-ARF7-1F	GGGGACAAGTTTGTACAAAAAAGCAGGCTTCATGAAAGCTCCTTCATCA
	attB2-GFP-720R	GGGGACCACTTTGTACAAGAAAGCTGGGTATTACTTGTACAGCTCGTCC
ChIP-pRSL4	Frag-1F	CTTTTCACATGCCCATAACTAG
	Frag-1R	GGTATTGTAGTTGTATACTTGTATGTA
	Frag-2F	TCTTCCCTTCTAGTGTTGTATGG
	Frag-2R	AGCTCATTTTAAACACAAAATGTTAC
	Frag-3F	ACAGCTGTATGTTTTTGGTATC
	Frag-3R	ACTCATTCGTAAGAGAGTGATC
	Frag-4F	TATATCATGCTGCCTCCAAA
	Frag-4R	CCATGCCGCTTTTTACCTTA
	Frag-5F	TTGCGATAATGATTCCACAA
	Frag-5R	TTTACATTGGCCACACAAGAG
	Frag-6F	GAGATGAATGGATAGTTATAAATAAGAAT
	Frag-6R	GATGAACACGATCAGTCAAC
	Frag-7F	TGGCTTCGTTTCACTTATTT
	Frag-7R	AGAGATCAAGAGATTCTTAAACTG
	Frag-8F	AAATCTTCCTTGAGAAATATTCTCT
	Frag-8R	TTCTTGAACTTGTGCAACTATAT
	Frag-9F	ATTCTTGGGATCAAAGTCATCACC
	Frag-9R	GTAAACATTATATATTGGATCTTCCAC
ChIP-pRBOHC	RBOHC ChIP1-F	TCCATGTGAAGAAAAATAGAAAGA
	RBOHC ChIP1-R	TGGCGTAAATAAAATTAGTAAATTAAG
	RBOHC ChIP2-F	CCGTAATGTTTGTGGAGTT
	RBOHC ChIP2-R	ATAGTAATTCTTATGTTTGTCCAAA

	RBOHC ChIP3-F	CAAATGCACGTTACAACCT
	RBOHC ChIP3-R	GAATGAGAAAATGGATTCGTAT
	RBOHC ChIP4-F	AAGTTCATTAGTAAAACCGAC
	RBOHC ChIP4-R	CTACAATACCAAATTTTCATTCAAT
ChIP-pRBOHH	RBOHH ChIP1-F	TTCCATTTGATATGACAAGTTG
	NADPoxH ChIP1-R	CACTGCTCCAATAATGTTTG
	RBOHH ChIP2-F	CTTTGTCCGAATTGTACAAAA
	RBOHH ChIP2-R	AGGTCAGAAGTTGCTGATA
	RBOHH ChIP3-F	CTAAAGGTACGAGTTTGGA
	RBOHH ChIP3-R	ACAATATACTTTCAACACAAAAATC
	RBOHH ChIP4-F	CATCAGCCGCACCTTC
	RBOHH ChIP4-R	GTGTTTTGTTTATTTAGTTACACATG
ChIP-pRBOHJ	RBOHJ ChIP1-F	AAACTGAGTATTCTCATTAACTATT
	RBOHJ ChIP1-R	TTATAAGTCGATCGAAGAGAA
	RBOHJ ChIP2-3F	GAAAAATTACCAAGTTATATATAATGGTGT
	RBOHJ ChIP2-R	TTGTAT ATCTCAGTATATGAGTG
	RBOHJ ChIP3-F	CGTTTGATCTTCCTTTGTTATAAA
	RBOHJ ChIP3-R	CTATGAGAAGAGACTAAGAATAG
ChIP-pPER3	PER3 ChIP1-F	AAGTCAATGAAATATCACTTTTTTCA
	PER3 ChIP1-R	ATTTCTCTATATATTCGCGTGATA
	PER3 ChIP2-F	TTCGTACTCTCCTACTAAAAAAAA
	PER3 ChIP2-R	TAAATATTTGAGACTTACGAGGAT
	PER3 ChIP3-F	TTTCACAAGAAACTAGCCGTA
	PER3 ChIP3-R	CTATTGACTTTGGAGAAGATGTA
	PER3 ChIP4-F	ATATGAAAAAACTAGCTAGTCCTAA
	PER3 ChIP4-R	AAGAAATGAGATTAGGACACTTC
ChIP-pPER44	PER44 ChIP1-F	AGCTTTTTCTTAATTGAATAAGTTTAAG
	PER44 ChIP1-R	ATGTAAAACTACAAATATGGAATGATT
	PER44 ChIP2-F	GACATAGACGTGGTATCCTTT
	PER44 ChIP2-R	ATTGACATTTGACGGGTTAGAG
	PER44 ChIP3-F	AATCTATCGTGGCTAGTGTTG
	PER44 ChIP3-R	CTACACAACCATTCAAAACATTG
ChIP-pPER60	PER60 ChIP1-F	ATTGTTGATTCAAAACCCTAATTAGA
	PER60 ChIP1-R	AATCAGTAGTATTCTCTTTTTTTTTGT
	PER60 ChIP2-F	TAATGTTTACAAGTCCTTATCACTT
	PER60 ChIP2-R	ACTGGCTCAACATAGGGATTAT
	PER60 ChIP3-F	TTTTATTATAAAATAGAACCAGCCC
	PER60 ChIP3-R	TAGAAAAATTGTTAACAACTTTTATAGTGT
	PER60 ChIP4-F	AAAACATCGTATCTAAAGTTGTTGG
	PER60 ChIP4-R	ATACAACAAATTAAAGATCAATATTTATTTC
ChIP-pPER73	PER73 ChIP1-F	TCACGGCCTTCTGAAATTCT

	PER73 ChIP1-R	AAAAAAGTTAAGGGACGTTTGATAAAAT
	PER73 ChIP2-F	AAAATAAAATGATTCAAAAACTACATCAAA
	PER73 ChIP2-R	TAAAAGGGTCTTTATGAGCAAC
	PER73 ChIP3-F	AACGCTTAAATATGTCATATTCTTTTA
	PER73 ChIP3-R	AAATGGAAGTTATCAATAAAATGATAG
	PER73 ChIP4-F	AATGTTGAACAAATCGTGAAAAAAGT
	PER73 ChIP4-R	TATTTATACATACCAACCAAAATTTTTAA
qRT-PCR	RSL4-qF842	GTGCCAAACGGGACAAAAGT
	RSL4-qR1097	TTGTGATGGAACCCCATGTC
	ARF5-qRT-F	TGAACAGCGCAGGCATTAAC
	ARF5-qRT-R	TACAGGCGCGCCGTTTCTCCTCTACCAGTTGG
	ARF7-qRT-F	CGGAGTTCTTGCAGCTGCAG
	ARF7-qRT-R	CACCAGCAGCTGACTCATCC
	ARF8-qRT-F	GATCATGGAGAAGGCAGTGG
	ARF8-qRT-R	GAATGGCGCGCCAAGATGAGTGGAAACGA
	ACT7-qRT-F	TCCCTCAGCACCTTCCAACAG
	ACT7-qRT-R	CAATTCCCATCTCAACTAGGG
RT-PCR	PER1 RT-F	GAAAGAGACGCTGTCCCCAA
	PER1 RT-R	CTGAGCCACGACCTTGAAGT
	PER44 RT-F	CTTGCTCCTTCTGCTTTGGC
	PER44 RT-R	CTCACGCTTGCATTTGGTCC
	PER73 RT-F	AGAGGACATGATCGCTCTTTCAGC
	PER73 RT-R	CGTCTAGTCTTAACGCCAACGC,
	PP2A RT-F	GTCGACCAAGCGGTTGTGGAGA
	PP2B RT-R	ACGCCCAACGAACAAATCACAGA
Promoter ARF5	ProARF5-SlF	TTAAGTCGACATATATCTTAGTGACAAACGCG
	ProARF5-KpR	TTAAGGTACCACAGAGAGATTTTTCAATG
GUS	GUS-PcF	ATATTTAATTAAATGTTACGTCCTGTAGA
	GUS-AvR	ATATCCTAGGACGGTGGCGATGGATCTTTGTTTGCCTCCCTGCTGCG
GFP	GFP-AvF	ATATCCTAGGTATGGTGAGCAAGGGCGAGGA
	GFP-AcR	AAGGCGCGCCATTACTTGTACAGCTCGTCC

References

1. V.V. Belousov *et al.* Genetically encoded fluorescent indicator for intracellular hydrogen peroxide. *Nat. Methods* **3,** 281-286 (2006).
2. A. Costa *et al.* H2O2 in plant peroxisomes: an in vivo analysis uncovers a Ca2+-dependent scavenging system. *Plant J.* **62,** 760-772 (2010).
3. N.M. Mishina *et al.* Visualization of intracellular hydrogen peroxide with HyPer, a genetically encoded fluorescent probe. *Methods Enzymol.* **526,** 45-59(2013).
4. A. Hernández-Barrera *et al.* HyPer, a Hydrogen Peroxide Sensor, Indicates the Sensitivity of the Arabidopsis Root Elongation Zone to Aluminum Treatment. *Sensors* **15,** 855-867 (2015).
5. T.L. Bailey *et al.* MEME SUITE: tools for motif discovery and searching. *Nucleic Acids Res.* **37,**W202-W208(2009).
6. R. Wang, M. Estelle. Diversity and specificity: auxin perception and signaling through the TIR1/AFB pathway. *Curr. Opin. Plant Biol.* **21**, 51–58(2014).
7. O.R. Lee *et al.* PINOID positively regulates auxin efflux in Arabidopsis root hair cells and tobacco cells. *Plant Cell* **22,** 1812–1825 (2010)
8. M.D. Curtis, U. Grossniklaus. A gateway cloning vector set for high-throughput functional analysis of genes in planta. *Plant Physiol.* **133**, 462-469 (2003).
9. A.-V. Gendrel, Z. Lippman, C. Youdan, V. Colot, R. Martienssen. Dependence of Heterochromatic Histone H3 Methylation Patterns on the Arabidopsis gene DDM1. *Science* **297**, 1871-1873 (2002).
10. M.-J. Kang, H.-S. Jin, Y.-S. Noh, B. Noh. Repression of flowering under a noninductive photoperiod by the HDA9-AGL19-FT module in Arabidopsis. *New Phytol.* **206**, 281-294 (2015).
11. B. Noh *et al.* Divergent roles of a pair of homologous jumonji/zinc-finger-class transcription factor proteins in the regulation of flowering time. *Plant Cell* **16**, 2601-2613 (2004).
12. C.P. Moehs, E.F. McElwain, S. Spiker. Chromosomal proteins of *Arabidopsis thaliana. Plant Mol. Biol.* **11**, 507-515 (1988).
13. Y. Lee, M.C. Rubio, J. Alassimone, N. Geldner. A mechanism for localized lignin deposition in the endodermis. *Cell* **153**, 402-412 (2013).
14. M.A. Torres, J.I. Dangl, J.D. Jones. Arabidopsis gp91phox homologues AtrbohD and AtrbohF are required for accumulation of reactive oxygen intermediates in the plant defense response. *Proc. Nat. Acad. Sci. USA* **99,** 517-522 (2002).
15. M.A. Torres, J.I. Dangl. Functions of the respiratory burst oxidase in biotic interactions, abiotic stress and development. *Curr. Opin. Plant Biol.* **8,** 397-403 (2005).
16. H.-T.Xie, Z.-Y. Wan, S. Li, Y. Zhang. Spatiotemporal Production of Reactive Oxygen Species by NADPH Oxidase Is Critical for Tapetal Programmed Cell Death and Pollen Development in Arabidopsis. *Plant Cell* **26**, 2007-2023 (2014).
17. A. Boisson-Dernier *et al.* ANXUR receptor-like kinases coordinate cell wall integrity with growth at the pollen tube tip via NADPH oxidases. *PLoS Biol.* **11**, e1001719 (2013).

18. R.C. Foley, C.A. Gleason, J.P. Anderson, T. Hamann, K.B. Singh. Genetic and Genomic Analysis of Rhizoctonia solani Interactions with *Arabidopsis*; Evidence of Resistance Mediated through NADPH Oxidases. *PLoS One* **8**, e56814. doi:10.1371/journal.pone.0056814 (2013).

19. Rademacher, E.H., Möller, B., Lokerse, A.S., Llavata-Peris, C.I., van den Berg, W., and Weijers, D. (2011). A cellular expression map of the *Arabidopsis AUXIN RESPONSE FACTOR* gene family. *Plant J.* 68,597–606.